~~Not accounting for~~ Ignoring carbon emissions from thermokarst ponds ~~leads to~~ results in overestimation of tundra carbon uptake

Lutz Beckebanze[1,2,*], Zoé Rehder[3,4,*], David Holl[1,2], Christian Wille[5], Charlotta Mirbach[1,2], and Lars Kutzbach[1,2]

[1]Institute of Soil Science, Universität Hamburg, Germany
[2]Center for Earth System Research and Sustainability (CEN), Universität Hamburg, Germany
[3]Department of the Land in the Earth System, Max Planck Institute for Meteorology, Hamburg, Germany
[4]International Max Planck Research School on Earth System Modeling, Hamburg, Germany
[5]Helmholtz-Zentrum Potsdam – Deutsches Geo Forschungs Zentrum (GFZ), Potsdam, Germany
[*]These authors contributed equally to this work.

Correspondence: Lutz Beckebanze (lutz.beckebanze@uni-hamburg.de), Zoé Rehder (zoe.rehder@mpimet.mpg.de)

Abstract. Arctic permafrost landscapes have functioned as a global carbon sink for millennia. These landscapes are very heterogeneous, and the omnipresent water bodies ~~are~~ within them act as a carbon source~~within them~~. Yet, ~~only a few studies focus~~ few studies have focused on the impact of these water bodies on the landscape carbon budget. We deepen our understanding of carbon emissions from thermokarst ponds and constrain their impact by comparing carbon dioxide and methane fluxes from these ponds to fluxes from the surrounding tundra. We use eddy covariance measurements from a tower located at the border between a large pond and semi-terrestrial tundra.

When ~~taking~~ we take the open-water areas of thermokarst ponds into account, ~~the carbon dioxide sink strength of the landscape is reduced by~~ our results show that the estimated summer carbon uptake of the polygonal tundra is 11~~%. Open-water~~ % lower. Further, the data show that open-water methane emissions are of similar magnitude as polygonal tundra emissions. However, some parts of the pond's shoreline exhibit much higher emissions. This finding underlines the high spatial variability of methane emissions. We conclude that gas fluxes from thermokarst ponds can contribute significantly to the carbon budget of arctic tundra landscapes. Consequently, changes in ~~arctic hydrology and the concomitant changes in the~~ the water body distribution of tundra landscapes due to permafrost degradation may substantially impact the overall carbon budget of the Arctic.

1 Introduction

Water bodies make up a significant part of the arctic lowlands with an areal coverage of about 17 % (Muster et al., 2017), and act as an important carbon source in a landscape that is ~~otherwise a~~ an overall carbon sink (Kuhn et al., 2018). ~~Permafrost thaw caused by~~ Intensified permafrost thaw in the warming Arctic will change the distribution of ~~waterbodies (Andresen and Lougheed, 2015; Br and thus also their contribution to the landscape-carbon budget (Kuhn et al., 2018)~~ water bodies, and thereby change their contribution (Andresen and Lougheed, 2015; Bring et al., 2016) to the landscape carbon budget (Kuhn et al., 2018) of tundra

landscapes. However, data on ~~greenhouse-gas~~ greenhouse gas emissions from arctic water bodies are still sparse~~in space and time~~, especially data with ~~a~~ high temporal resolution and from non-Yedoma regions (Vonk et al., 2015).

Our study site ~~,~~ in the Lena River Delta, Siberia, is located on an island mostly ~~covered~~ characterized by non-Yedoma polygonal tundra (Fig. 1). This landscape features many ponds~~, which are defined here by an area $< 8 \cdot 10^4$~~ ; we define ponds as water bodies with an area of less than $8 \cdot 10^4$ m^2, ~~Ramsar Convention Secretariat (2016); Rehder et al. (2021). In following Ramsar Convention Secretariat (2016); Rehder et al. (2021).~~ Within our area of interest, ponds cover about ~~as much~~ the same area as lakes (Abnizova et al., 2012; Muster et al., 2012). The ponds ~~in this polygonal tundra~~ on Samoylov Island have formed almost exclusively through thermokarst processes: The ~~ground~~ soil has a high ice content, so when the ice melts, the ground subsides, and thermokarst ponds form (Ellis et al., 2008). These thermokarst ponds are often only as ~~big~~ large as one polygon ~~, but when~~ (polygonal ponds). When several polygons are inundated, ~~larger shallow water bodies~~ this can cause larger shallow thermokarst ponds to form, which we ~~call~~ term merged polygonal ponds (Rehder et al., 2021). ~~Ponds~~ Holgerson and Raymond (2016) as well as Wik et al. (2016) report that ponds emit more greenhouse gases per unit area than lakes~~(Holgerson and Raymond, 2016; Wik et al., 2016)~~, defined here as water bodies with an area larger than $8 \cdot 10^4$ m^2. Thus, in our study area, they have a ~~higher~~ greater potential than lakes to counterbalance the carbon ~~sink function~~ uptake of the surrounding tundra (McGuire et al., 2012; Jammet et al., 2017; Kuhn et al., 2018). To better understand the impact of thermokarst ponds on the landscape carbon flux, we compare carbon dioxide (CO_2) and methane (CH_4) fluxes from ~~the open-water area of~~ thermokarst ponds to fluxes from the semi-terrestrial tundra~~, which we define as~~ . The semi-terrestrial tundra consists of wet and dry tundra, and overgrown ~~water~~shallow water, which are the terrestrial land-surface types used by Muster et al. (2012) to classify Samoylov Island.

The main ~~driving~~ geophysical and biochemical processes ~~differ between CO_2 and~~ that drive CH_4 ~~emissions. On the one hand,~~ fluxes are different to the ones that drive CO_2 fluxes. The microbial decomposition of dissolved organic carbon, which is introduced laterally into the aquatic system through rain and meltwater (Neff and Asner, 2001), dominates aquatic CO_2 production. When supersaturated with dissolved CO_2, ponds emit CO_2 ~~to~~ into the atmosphere through diffusion. While photosynthetic CO_2 uptake has been observed in some clear arctic water bodies (Squires and Lesack, 2003), most arctic water bodies are net CO_2 sources (Kuhn et al., 2018). Estimates ~~range from emissions~~ of CO_2 emissions range from close to zero (0.028 g m^2 d^{-1} by Treat et al. (2018), ~~or~~ and 0.059 g m^2 d^{-1} by Jammet et al. (2017)) to substantial ~~CO_2-C emissions~~ (1.4~~– 2.2~~ –2.2 g m^2 d^{-1} by Abnizova et al. (2012)).

~~On the other hand~~Within just one site, CH_4 emissions ~~vary even more, sometimes~~ from a water body can vary by up to five orders of magnitude~~within just one site~~: 0.5~~– 6432~~ –6432 mg m^2 d^{-1} ~~, Bouchard et al. (2015).~~ (Bouchard et al., 2015) . The CH_4 that ponds emit is mostly produced in sub-aquatic soils and anoxic bottom waters (Conrad, 1999; Hedderich and Whitman, 2006; Borrel et al., 2011). Additionally, CH_4 ~~can~~ might also be produced in the oxic water column (Bogard et al., 2014; Donis et al., 2017), though this ~~pathway only becomes~~ location of methanogenesis is only significant in large water bodies (Günthel et al., 2020)~~and is still under debate (Encinas Fernández et al., 2016; Peeters et al., 2019). Note that during methanogenesis,~~ . Moreover, there is still ongoing debate as to whether methanogensis occurs in oxic waters at all (Encinas Fernández et al., 2016; Peeters et al., 2019). CO_2 is also formed as a byproduct ~~(Hedderich and Whitman, 2006)~~

. of the methanogensis process (Hedderich and Whitman, 2006). Water bodies emit CH_4 is then emitted from water bodies produced in their benthic zone through diffusion, ebullition (sudden release of bubbles), and or plant-mediated transport. These three The varying contributions of these three local methane emissions pathways lead to high spatial variability between water bodies and within one a single water body (Sepulveda-Jauregui et al., 2015; Jansen et al., 2019). Especially In particular, local seep ebullition causes high spatial variance of CH_4 emissions within one water body when it occurs (Walter et al., 2006) . Varying (Walter et al., 2006). Variability in the coverage and composition of vascular plants within the shallow parts of plant communities in a water body can also increase CH_4 variability because each plant species has its specific efficiency in transporting CH_4 transport efficiency can be species-specific (Knoblauch et al., 2015; Andresen et al., 2017).

To study spatial and temporal patterns , we analyze of carbon emissions from thermokarst ponds, we analyzed land-atmosphere CO_2 and CH_4 flux observations from an eddy-covariance eddy covariance (EC) tower on Samoylov Island, Lena River Delta, Russia. We set up the EC tower up within the polygonal tundra and next to a landscape at the border between a large merged polygonal pond and the surrounding semi-terrestrial tundra for two months in summer 2019. The polygonal structures are were still clearly visible along the shore and underwater, and the pond is mostly most of the pond was shallow (Rehder et al., 2021). Due to the tower's position, fluxes from the merged polygonal pond are were the dominant source of the observed EC fluxes under easterly winds. The From other wind directions, the observed EC fluxes are were dominated by semi-terrestrial polygonal tundra with only a low influence from small thermokarst pondsfrom the other wind directions. We aim to deepen our polygonal ponds. This paper aims to deepen the understanding of carbon emissions from thermokarst ponds and constrain their impact on the landscape carbon balance. To this end, we We (1) compare the water body and tundra fluxes focusing on examine the temporal and spatial patterns , and we of NEE and the spatial pattern of CH_4 flux from semi-terrestrial tundra and thermokarst ponds, and (2) investigate the influence of the merged polygonal pond thermokarst ponds on the landscape carbon balanceNEE of CO_2 during the months June to September 2019. To this end, we use a footprint model and model net ecosystem exchange (NEE) of CO_2 using the footprint weights of semi-terrestrial tundra and thermokarst ponds.

2 Methods

2.1 Study site

Samoylov Island (72°22'N, 126°28'E) lies is located in the southern part of the Lena River Delta (Fig. 1, b). It has a size of about is approximately five km^2 large and consists of two geomorphologically different unitscomponents. The western part of the island (∼2 km^2) is a floodplainannually flooded in , which is flooded annually during the spring. The eastern part of the island (∼3 km^2), a late-Holocene river terrace, is characterized by polygonal tundra. The partially degraded polygonal tundra at this study site features a high spatial heterogeneity within a few meterson a scale of a few meters in several aspects, including vegetation, water table height, and soil properties. Dry and wet vegetated parts of the semi-terrestrial tundra are interspersed with small and large thermokarst ponds (<1 m^2 – 1–>10000 10,000 m^2) and with large thermokarst larger lakes (up to 0.05 km^2, Boike et al. (2015a); Kartoziia (2019)). The island is surrounded by the Lena River and sandy floodplains, creating more additional spatial heterogeneity on a larger scale.

~~We focus~~ This study focuses on a merged polygonal pond (Fig. 1, d, and A1) ~~in~~ on the eastern part of the island. This merged polygonal pond has a size of 0.024 km^2 with a maximum depth of 3.4 meters and a mean depth of 1.2 meters (Rehder et al., 2021; Boike et al., 2015a). ~~On~~ In an aerial image of the pond, the polygonal structures are ~~still~~ clearly visible under the water's surface (Boike et al., 2015c). The vegetated shoreline of this merged polygonal pond is dominated by *Carex aquatilis*~~interspersed with~~, but it also features *Carex chordorrhiza*, *Potentilla palustris*, and *Aulacomnium spp.*. These plants grow in the water ~~close to~~ near the shore while the deeper parts of the merged polygonal pond are vegetation-free.

2.2 Instruments

We ~~measure~~ measured gas fluxes using an eddy covariance (EC) tower between July 11 and September 10, 2019. The EC tower ~~is~~ was located on the eastern part of Samoylov Island, directly at the western shore of the merged polygonal pond (Fig. 1, d). The EC instruments ~~are~~ were mounted on a tripod at ~~the~~ a height of 2.25 meters (Fig. A1). The tower ~~is~~ was equipped with an enclosed-path CO_2/H_2O sensor (LI-7200, LI-COR Biosciences, USA), an open-path CH_4 sensor (LI-7700, LI-COR Biosciences, USA), and a 3D-ultrasonic anemometer (R3-50, Gill Instruments Limited, UK). All instruments ~~have~~ had a sampling rate of 20 Hz. We also ~~install~~ installed radiation-shielded temperature and humidity sensors at the EC tower (HMP 155, Vaisala, Finland) and ~~use~~ used data from a photosynthetically active radiation (PAR) sensor mounted ~~at~~ on a tower approximately 500 meters to the west of the EC tower (SKP 215, Skye Instruments, UK). Additional meteorological data for Samoylov Island ~~is~~ was provided by Boike et al. (2019).

2.3 Data processing

~~We perform~~

We performed the raw data processing and computation of half-hourly fluxes for open-path and enclosed-path fluxes (CO_2, CH_4 and H_2O) using *EddyPro 7.0.6* (LI-COR, 2019). The convention of this software is that positive fluxes are fluxes from the surface to the atmosphere, while negative fluxes indicate a flux from the atmosphere downwards. Raw data screening ~~includes~~ included spike detection and removal according to Vickers and Mahrt (1997) (1 % maximum accepted spikes and a maximum of three consecutive outliners). Additionally, we ~~apply~~ applied statistical tests for raw data screening, including tests for amplitude resolution, skewness and kurtosis, discontinuities, angle of attack, and horizontal winds steadiness. All ~~parameters~~ of these tests~~are~~ ' parameters were set to *EddyPro* default values. We ~~rotate~~ rotated the wind-speed axis to a zero-mean vertical wind speed using ~~the~~ Kaimal and Finnigan's (1994) "double rotation" ~~method by Kaimal and Finnigan (1994). We apply~~ method. Further, we applied linear de-trending ~~following Gash and Culf (1996)~~ to the raw data ~~before~~ following Gash and Culf (1996) before performing flux calculations. We ~~compensate time lags by automatic time-lag~~ compensated time lags via automatic time lag optimization using a ~~time-lag-assessment~~ time lag assessment file from a previous EddyPro run. In this previous ~~time-lag~~ time lag assessment, the time lags for all gases ~~are detected by~~ were detected using covariance maximization (Fan et al., 1990), resulting in time lags between ~~0 – 0.4~~ 0–0.4 s for CO_2 and -0.5–+0.5 s for CH_4. For H_2O, the time lag ~~is~~ was humidity-dependent and ~~is calculated for ten~~ was calculated for 10 humidity classes. We ~~compensate~~ compensated for air-density fluctuations due to thermal expansion ~~/~~and contraction and varying water-vapor concentrations, following Webb et al.

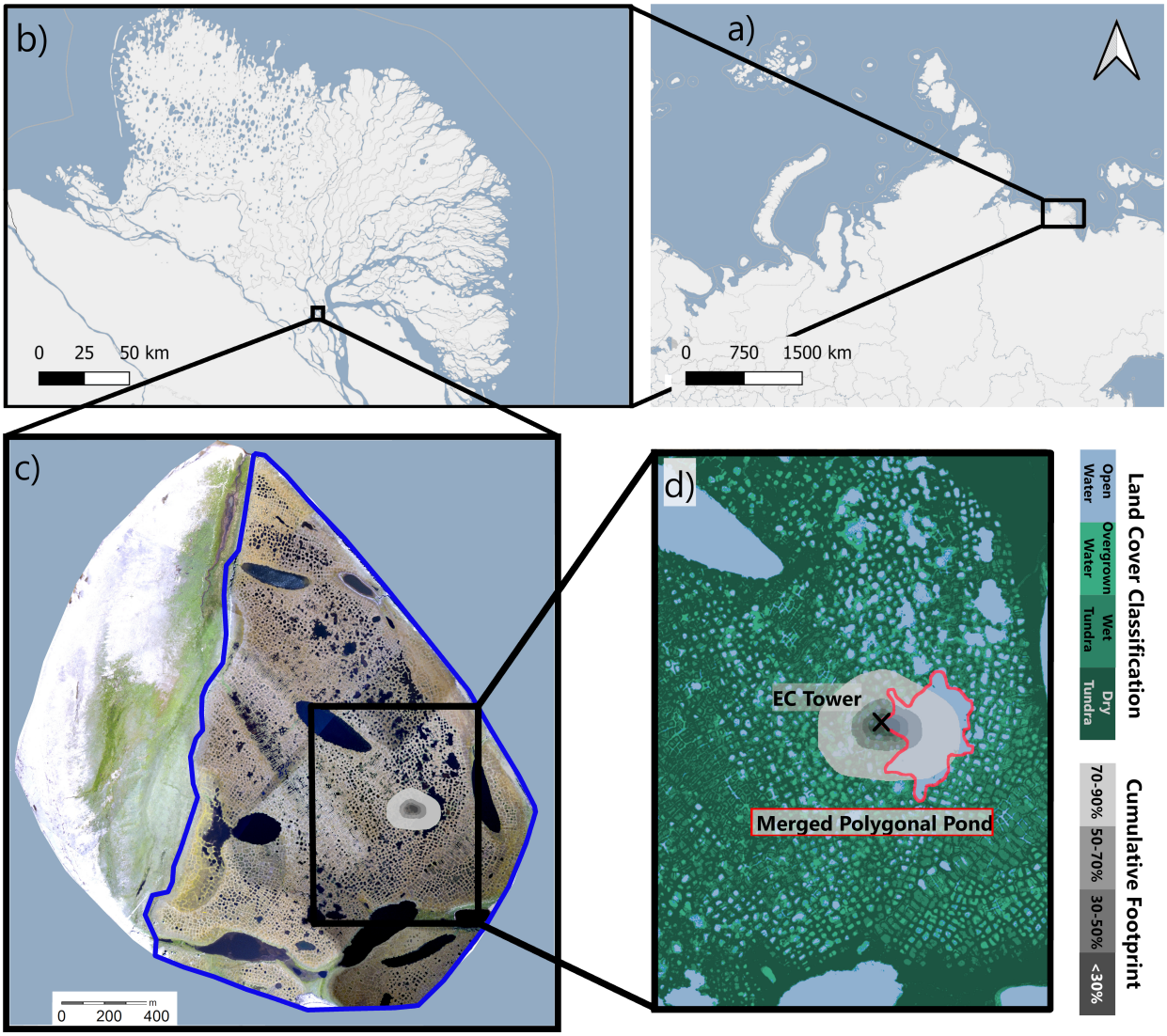

Figure 1. ~~Study site with an overview~~ The location of the study site in Russia is shown in (a) ~~,~~ and the location of Samoylov Island within the Lena River Delta is shown in (b)~~,~~. Samoylov Island ~~with~~ is shown in (c); the surrounding Lena River appears in light blue~~(c), and a close-up look at the study site (d)~~. The ~~EC tower is marked as a black cross with the cumulative footprint (see section 2.4.2) in gray shades surrounding the EC tower. The~~ outline of the ~~land cover~~ river-terrace land-cover classification ~~from section~~ (Sect. 2.4.1) is ~~shown in a~~ indicated by the blue line. We focus on the polygonal tundra, however, large lakes are excluded (~~e~~circled in yellow). In (d), the ~~detailed land cover~~ land-cover classification is ~~shown~~ drawn in blue (open water) and green shades (dark green: dry tundra~~,~~; medium green: wet tundra~~,~~; and light green: overgrown water). The merged polygonal pond studied here is outlined in red. The location of the EC tower is marked by a black cross. The cumulative footprint (see Sect. 2.4.2) is shown in gray shades. 30 % of the flux likely originated from within the dark gray area, 50 % from within the medium-dark gray area, 70 % from within the medium-light gray area and 90 % from within the light gray area. Map data from © OpenStreetMap contributors 2020, distributed under the Open Data Commons Open Database License (ODbL) v1.0 (a & b) and modified ~~after~~ based on Boike et al. (2012) (c & d).

(1980). This correction depends on accurate measurements of the latent and sensible heat flux and ~~is~~ was applied to the open-path data of the LI-7700. ~~Especially for~~ For the LI-7700 in particular, the correction term can be larger than the flux itself, but the correction ~~is~~ was derived from the underlying physical equations. ~~By using~~ Because we used well-calibrated instruments as well as *EddyPro*, which uses an up-to-date implementation of the correction, ~~and by using well-calibrated instruments, we are certain to receive~~ we were confident that the LI-7700 would provide accurate CH_4 flux ~~estimations from the LI-7700~~estimates. For enclosed-path data, we ~~perform~~ performed a sample-by-sample conversion into mixing ratios to account for ~~air-density~~ air density fluctuations (Ibrom et al., 2007b; Burba et al., 2012). Flux losses ~~occur~~ occurred in the low- and ~~high-frequency~~ high frequency spectral range due to different filtering effects. ~~In the low-frequency range, we compensate flux losses following~~ We compensated flux losses in the low-frequeny range in accordance with Moncrieff et al. (2004) and in the high-frequency range ~~following~~ in accordance with Fratini et al. (2012). For ~~applying the latter~~ the high-frequency range compensation method, a spectral assessment file ~~is created using the methodby Ibrom et al. (2007a)~~was created using Ibrom et al.'s (2007a) method. The spectral assessment ~~results~~ resulted in cut-off frequencies of 3.05 Hz and 1.67 Hz for CO_2 and CH_4, respectively. For H_2O, we ~~find~~ found a humidity-dependent cut-off frequency between 1.25 Hz (RH ~~5 - 45~~5–45 %) and 0.21 Hz (RH ~~75 - 95~~75–95%). We ~~perform~~ performed a quality check on each half-hourly flux following the 0-1-2 system proposed by Mauder and Foken (2004). In this quality check, flux intervals with the lowest quality ~~receive~~ received the flag "2" and ~~are~~ were excluded from further analysis.

2.4 Data analysis

2.4.1 ~~Land cover~~ Land-cover classification

The ~~land cover~~ land-cover classification covers the late-Holocene river terrace of Samoylov Island ~~.~~ (3.0 km^2, area within the blue line in Fig. 1, c). It is based on high-resolution near-infrared (NIR) orthomosaic aerial imagery obtained in the summer of 2008 (Boike et al., 2015b). We ~~use~~ used a subset of ~~the existing classification by Muster et al. (2012)~~ Muster et al.'s (2012) existing classification as a training dataset to perform a semi-supervised ~~land cover~~ land-cover classification using the *maximum likelihood algorithm* in ArcMap Version 10.8 (ESRI Inc, USA). We then ~~apply~~ applied the ArcMap *majority filter* tool to the new classification. The ~~land cover~~ land-cover classification has a resolution of 0.17 m x 0.17 m,~~it~~ . It is projected onto WGS 1984 UTM Zone 52N and the land-cover classes include *open water* (15.7 %), *overgrown water* (7.0 %), *dry tundra* (65.1 %), and *wet tundra* (12.1 %), as defined by Muster et al. (2012). We summarize the classes *overgrown water*, *dry tundra*, and *wet tundra* in the land-cover type, semi-terrestrial tundra. The river terrace consists of this semi-terrestrial tundra, large lakes, and thermokarst ponds. Since small ponds are an integral part of the polygonal tundra, we use the term "polygonal tundra" to refer to the area of the river terrace covered by semi-terrestrial tundra and by thermokarst ponds.

2.4.2 Footprint model

~~The tower~~In deploying an EC measurement tower, the tower's location and sensor height are crucial parameters~~in deploying an EC measurement tower~~. A lower measurement height results in a smaller footprint. The tower's footprint describes the

source area of the flux ~~from~~ within the surrounding landscape. ~~With our sensors installed at the~~ As we installed sensors at a height of 2.25 m next to the merged polygonal pond, we ~~expect~~ expected to observe substantial flux signals from the adjacent water body as well as from the surrounding ~~polygonal~~ semi-terrestrial tundra. Each ~~land cover~~ land-cover type's contribution to the flux signal ~~depends~~ depended on the wind direction and turbulence ~~in the atmospheric boundary layer. We implement~~ characteristics. We implemented the analytical footprint model proposed by Kormann and Meixner (2001) in Matlab 2019b (MATLAB, 2019). We ~~combine~~ combined the footprint model with ~~land cover~~ land-cover classification data described in ~~section~~ Sect. 2.4.1 to estimate the contribution of each ~~land cover~~ land-cover type to each ~~flux signal~~ half-hourly flux (from now on referred to as the weighted footprint fraction). The model ~~accounts~~ accounted for the stratification of the atmospheric boundary layer and ~~requires~~ required a height-independent crosswind distribution and horizontal homogeneity of the surface. The input data ~~requires~~ required stationarity of atmospheric conditions during the flux intervals of 30 minutes. ~~We derive~~

We derived the vertical power-law profiles for the eddy diffusivity and the wind speed for each 30-minute flux depending on the atmospheric stratification (~~equation~~ see Eq. 6 in Kormann and Meixner (2001)). We ~~use~~ used an analytical approach to find the closest Monin-Obukhov (M-O) similarity profile (~~equation~~ see Eq. 36 in Kormann and Meixner (2001)). Next, we ~~calculate~~ calculated a two-dimensional probability density function of the source area for each flux (from ~~equations~~ Eq. 9 and 21 in Kormann and Meixner (2001)). We ~~combine~~ combined each probability density function with the ~~land cover classification of the river terrace of Samoylov Island,~~ land-cover classification of Samoylov Island's river terrace with its four ~~land cover~~ land-cover types (see ~~section~~ Sect. 2.4.1). The resolution of the footprint model ~~is~~ was set to the ~~land cover~~ land-cover classification resolution of 0.17 m x 0.17 m. Hence, we ~~can~~ were able to estimate how much a given grid cell ~~contributes~~ contributed to each 30-min flux. We also ~~know~~ knew each grid cell's dominant ~~land cover~~ land-cover type from the ~~land cover~~ land-cover classification. We ~~combine both~~ combined both pieces of information for each grid cell and ~~calculate~~ calculated the sum of the fraction fluxes within the source area for each of the four land-cover types (*dry tundra*, *wet tundra*, *overgrown water*, and *open water*) and ~~obtain~~ determined the contribution of each ~~land cover type to~~ land-cover type in respect of each 30-minute flux ($a_{dry\ tundra}$, $a_{wet\ tundra}$, $a_{overgrown\ water}$, and $a_{open\ water}$). We refer to this contribution of each ~~land cover~~ land-cover type as the *weighted footprint fraction*.

We also ~~sum~~ summed all 30-min two-dimensional probability density functions over the ~~whole~~ entire deployment time. This sum is referred to as the cumulative footprint (gray shaded area in Fig. 1, c–d). ~~The light gray area's outer boundary represents the 90% isoline, and the light gray area's inner boundary is the 70% isoline of the cumulative footprint. The 90% isoline means that it is likely that 10% of each observed flux signal originates from outside of the light gray area. Medium gray represents 50-70%, medium-dark gray 30-50%, and dark gray indicates a probability of less than 30% that each observed flux signal originates from within the marked area.~~

2.4.3 Gap-filling the CO_2 flux

To gap-fill the net-ecosystem exchange (NEE) fluxes of CO_2, we ~~use~~ used the *bulk-NEE model* proposed by Runkle et al. (2013). The model ~~uses the total ecosystem respiration (TER) and the gross primary production (GPP) to gap-fill NEE, our target variable. The model~~ is specifically designed to model NEE in arctic regions: It takes impacts of the polar day into account

~~. We estimate all model parameters for running 5-day periods to capture changing plant physiology during the measurement period. NEE is partitioned into two components (equation 1): TER(~~by allowing both respiration and photosynthesis to occur simultaneously throughout the day. The *bulk-NEE model* uses the sum of total ecosystem respiration (TER) and gross primary production (GPP) to describe NEE, our target variable:

$$NEE = \mathrm{TER} + \mathrm{GPP} \tag{1}$$

where TER and GPP have the unit ~~µmol m^{-2} s^{-1}, equation 2) and GPP (~~mol m^{-2} s^{-1}~~, equation 3). Parameters of both components are fit simultaneously. TER is modeled .~~ TER is approximated as an exponential function of air temperature T_{air}:

$$\mathrm{TER} = R_{base} \cdot Q_{10}^{\frac{T_{air} - T_{ref}}{\gamma}} \tag{2}$$

where $T_{ref} = 15$ °C and $\gamma = 10$ °C are constant, independent parameters. R_{base} (µmol m^{-2} s^{-1}) describes the basal respiration at the reference temperature T_{ref} and Q_{10} (dimensionless) describes the sensitivity of ecosystem respiration to air temperature changes.

GPP is ~~modeled~~ described as a rectangular hyperbolic function of PAR (µmol m^{-2} s^{-1}):

$$\mathrm{GPP} = -\frac{P_{max} \cdot \alpha \cdot \mathrm{PAR}}{P_{max} + \alpha \cdot \mathrm{PAR}} \tag{3}$$

where α (µmol µmol^{-1}) is the initial canopy quantum use efficiency (slope of the fitted curve at PAR$= 0$) and P_{max} (µmol m^{-2} s^{-1}) is the maximum canopy photosynthetic potential for PAR $\to \infty$.

~~We sum both components to estimate the modeled NEE $F_{CO_2,mod}$:~~

$F_{CO_2,mod} = \mathrm{TER} + \mathrm{GPP}.$

The parameters R_{base}, Q_{10}, P_{max}, and α were fitted simultaneously. To account for seasonal changes in plant physiology, we fitted the parameters for running five-day windows as proposed in Holl et al. (2019).

We split the datasets into ~~a~~ training (70 %) and ~~a~~ validation (30 %) data ~~set~~ sets to test model performance. ~~In 38 5-day fitting periods, we find an R^2 above 0.9 between the model output and the validation set. Eighteen times, we get an R^2 between 0.8 – 0.9 and six times an R^2 below 0.7. The model performance indicates that the model works well overall. In the model input, we exclude CO$_2$ fluxes with an absolute value of more than 4 g m^{-2} d^{-1}. We additionally exclude CO$_2$ fluxes from the wind direction (WD) of the merged polygonal pond (30°< WD <150°) from the training dataset to obtain a dataset consisting of as much semi-terrestrial tundra as possible. We perform this step since we expect little to no photosynthetic activity in the open-water part of the merged polygonal pond. We implement the *bulk model* in~~ We implemented the *bulk-NEE model* in Matlab 2019b (MATLAB, 2019) using the *fit* function with the ~~fitting method of *NonLinearLeastSquares*. We use *NonLinearLeastSquares* fitting method. We used~~ the *coeffvalues*-function to estimate the four parameters ~~and~~ (R_{base}, Q_{10}, P_{max}, and α) and the *confint*-function to estimate their 95 % confidence bounds. All partitioned fluxes ~~are~~ were converted into CO$_2$-C fluxes in the unit g m^{-2} d^{-1} before ~~the~~ data analysis.

2.4.4 ~~The open-water~~ Separating CO_2 ~~flux~~fluxes from semi-terrestrial tundra and water bodies

We ~~want~~ wanted to extract fluxes from thermokarst ponds and semi-terrestrial tundra to analyze the influence of ~~ponds on~~ thermokarst ponds on the carbon balance of a polygonal tundra landscape. However, due to the strong heterogeneity of the landscape and the relatively small size of the merged polygonal pond compared to the EC footprint, we ~~measure~~ measured a mixed signal from all wind directions. In other words, each flux that was measured with the EC method ~~contains~~ contained information from different ~~land-cover types. Since we are interested in average tundra fluxes, we combine the landcover classes dry tundra, wet tundra, and overgrown water under the term *semi-terrestrial tundra*. In this way, we can compare two landcover classes ,~~ land-cover types. We divided the footprint into two classes – semi-terrestrial tundra and ~~the open water from thermokarst ponds .~~ thermokarst ponds – to assess the impact of thermokarst ponds on the carbon balance.

Similar approaches of analyzing heterogeneous eddy covariance fluxes in arctic environments have been conducted for CO_2 and CH_4 (e.g. Rößger et al., 2019a,b; Tuovinen et al., 2019). Rößger et al. (2019a,b) extracted CO_2 and CH_4 fluxes from two different ~~land cover~~ land-cover classes on a floodplain, ~~and~~ while Tuovinen et al. (2019) separated CH_4 fluxes from nine individual ~~land cover~~ land-cover classes, including water, and combined them into four source classes (with no separate class for water). All three studies ~~have in common that they differentiate~~ differentiate between fluxes from different vegetation types. ~~However, our~~ Our method is dedicated to distinguishing between fluxes from semi-terrestrial tundra and water bodies.

To estimate ~~the~~ CO_2 ~~flux~~ fluxes from the merged polygonal pond (F_{pond}), we first ~~fit the~~ fitted the ~~*bulk*~~ *bulk-NEE model* to ~~data~~ training data, excluding fluxes from the direction of the merged polygonal pond (~~thus exclude fluxes from~~ 30° < WD < 150°~~, as described in section 2.4.3). With this bulk model, we gap-fill the CO_2 flux, and the~~). We obtained a dataset consisting of information about as much semi-terrestrial tundra as possible. We performed this step since we expected little to no photosynthetic activity in the open-water part of the merged polygonal pond. This gap-filled CO_2 flux (hereinafter $F_{modeled,mix}$) represents the ~~semi-terrestrial~~ polygonal tundra surrounding the EC tower, ~~including small ponds to the~~ meaning the flux is dominated by semi-terrestrial tundra, but also includes polygonal ponds from wind directions of north, west, and south. ~~Second, we assume~~ In the model input, we excluded 30-minute CO_2 fluxes with an absolute value of more than 4 g m^{-2} d^{-1}. In 38 five-day windows, we found an R^2 above 0.9 between the model output and the validation set. In 18 cases, we obtained an R^2 between 0.8–0.9; in six instances, we obtained an R^2 below 0.7. The final RMSE between the model input and the gap-filled NEE had a value of 0.29 g m^{-2} d^{-1}.

We assumed that the total observed flux ~~is~~ was a linear combination of the fluxes from the ~~land cover~~ land-cover types weighted by their respective contribution to the footprint. Thus, we ~~postulate~~ postulated that the observed CO_2 flux ($F_{obs,mix}$, not gap-filled) ~~is~~ was the sum of the individual ~~land cover~~ land-cover type fluxes ($F_{modeled,mix}$ and the merged polygonal pond F_{pond}) each multiplied with their weighted footprint fraction (~~a_{tundra}~~ a_{mix} and a_{pond}), with $a_{open\ water} = a_{pond}$,

$a_{tundra} = a_{sum} - a_{pond}$ $a_{mix} = a_{sum} - a_{pond}$, and a_{sum} is being the sum over all land cover classes: land-cover classes:

$$F_{obs,mix} = a_{pond} \cdot F_{pond} + a_{tundra\,mix} \cdot F_{modeled,mix}$$

$$\Leftrightarrow F_{pond} = \frac{F_{obs,mix} - a_{tundra} \cdot F_{modeled,mix}}{a_{pond}} \quad \frac{F_{obs,mix} - a_{mix} \cdot F_{modeled,mix}}{a_{pond}} \tag{4}$$

To improve data quality, we exclude excluded 30-min fluxes of F_{pond} when $a_{pond} < 50$ %. Then, we use used the median of F_{pond} for further calculations, and we assume that all open water assumed that all thermokarst ponds in the EC footprint emits emitted the same amount of CO_2.

As mentioned above, the observed CO_2 flux from the wind direction of north, west, and south ($F_{obs,mix}$) is still influenced by small thermokarst ponds. To analyze in detail the was influenced by polygonal ponds to a small degree. Since our aim was to assess the impact of thermokarst ponds (both polygonal ponds and merged polygonal ponds) on NEE, we needed to eliminate the influence of polygonal ponds from our NEE estimate. To extract uncontaminated CO_2 flux data from the semi-terrestrial tundra ($F_{modeled,tundra}$), we subtract subtracted the previously estimated pond COpond CO_2 flux F_{pond} from the observed CO_2 flux $F_{obs,mix}$:

$$F_{modeled,tundra} = \frac{F_{obs,mix} - a_{pond} \cdot F_{pond}}{a_{tundra}} \quad \frac{F_{obs,mix} - a_{pond} \cdot F_{pond}}{a_{mix}} \tag{5}$$

We then use used this estimated CO_2 flux from the semi-terrestrial tundra $F_{modeled,tundra}$ as the input regressand variable for the *bulk bulk-NEE model* to receive obtain a gap-filled dataset of regarding CO_2 flux from the semi-terrestrial tundra. This gap-filling modeling of CO_2-C flux had an RSME of 0.31 g m^{-2} d^{-1}.

To evaluate the impact of ponds on the thermokarst ponds on landscape CO_2 flux, we estimate a polygonal-tundra estimated a polygonal tundra landscape-CO_2 flux from the late-Holocene river terrace of Samoylov Island ($F_{landscape}$) by linearly combining combining thermokarst ponds and semi-terrestrial tundra linearly:

$$F_{landscape} = A_{pond} \cdot F_{pond} + A_{tundra} \cdot F_{modeled,tundra}$$

where F_{pond} describes the CO_2 emission emissions from the open-water areas of ponds (equation thermokarst ponds (Eq. 4), $F_{modeled,tundra}$ describes the modeled CO_2 flux from the semi-terrestrial tundra (equation Eq. 5), $A_{pond} = 0.07$ is the fraction of the coverage of open pond water on the whole river terrace river terrace area of Samoylov Island that is covered by thermokarst ponds (from the land cover classification, section land-cover classification, see Sect. 2.4.1) and $A_{tundra} = 1 - 0.07$ the coverage of other land cover types. We do is the fraction of other land-cover to the entire river terrace area. We did not account for (larger , deeper) thermokarst larger or deeper lakes in this up-scaling approach, as we expect expected different greenhouse gas emissions emission dynamics from these lakes and there are were no lakes in our footprint, and therefore not within our observation range. Thus, we scale scaled the above numbers to $A_{tundra} + A_{pond} = 1$, which results in $A_{pond} = 0.076$ and $A_{tundra} = 0.924$.

2.4.5 CH_4 flux partitioning

~~Since we do not have a simple~~ The data show that the CH_4 emissions from the heterogeneous landscape around the tower were less spatially uniform than the CO_2 emissions. Therefore, we could not use a gap-filling model ~~at hand~~ for CH_4 ~~emissions from the tundra, and since CH_4 emissions are much more variable than~~ that was similar to the bulk model we used for CO_2 ~~emissions, we treat~~ , so we investigated CH_4 ~~differently. We focus on~~ emissions in a different way. Based on preliminary results from our analysis and the aerial image of the study site, we focused on four wind sectors instead of extracting the fluxes from the ~~landcover types. We divide fluxes into the following wind sectors~~land-cover types:

- *tundra*: At least half of the footprint ~~consists~~ consisted of dry tundra, and the wind direction ~~is~~ was larger than 170°.
- $shore_{50°}$: Less than 40~~%~~ % of the footprint ~~consists~~ consisted of dry tundra and water ~~contributed to the footprint with at~~ comprised least 30~~%~~% of the footprint. The wind direction ~~lies~~ was between 30° < WD < 65°.
- *pond*: At least half of the footprint ~~consists~~ consisted of open water, and the wind direction ~~lies~~ was between 65° < WD < 110°.
- $shore_{120°}$: Less than 40~~%~~ % of the footprint ~~consists~~ consisted of dry tundra and water ~~contributed to the footprint with~~ comprised at least 30~~%~~% of the footprint. The wind direction ~~lies~~ was between 110° < WD < 130°.

2.4.6 CH_4 permutation test

To evaluate whether the differences in flux medians between the four wind sectors ~~are~~ were significant, we ~~apply~~ applied a permutation test (Edgington and Onghena, 2007). In this test, we randomly ~~assign~~ assigned each 30-min flux to one of two groups and ~~calculate~~ calculated both groups' median and ~~their differences . Using the four wind sectors, we do~~ the differences between the group's medians. We conducted six tests in total, using all possible combinations of pairs with the four wind sectors. After repeating this step 10000 times, we ~~plot~~ plotted the resulting differences in medians in a histogram and ~~perform~~ performed a one-sample t-test to evaluate whether the observed difference in medians ~~differs significantly (p<~~differed significantly ($p <$ 0.01) from the randomly generated differences.

3 Results

3.1 Meteorological conditions

During the measurement period between ~~11 July and 10 September~~ July 11 and September 10, 2019, half-hourly air temperatures range from -0.5 °C to 27.6 °C with a mean temperature of 8.7 °C (Fig. A2, a). The maximum wind speed measured ~~on~~ at the EC tower at a height of 2.25 m ~~height~~ is 8.9 m s^{-1} (Fig. A2, b). ~~Photosynthetically active radiation (PAR)~~ PAR reaches values of up to 1419 µmol m^{-2} s^{-1} with decreasing maximum values during the measurement period (Fig. A2, c). Throughout the measurement period, there are 28 cloudy days~~are visible as~~ , determined by identifying days with low PAR-values (maximum values below ∼500 µmol m^{-2} s^{-1})~~throughout the measurement period~~.

3.2 CO_2 fluxes

When inspecting the relation between observed CO_2 fluxes and wind direction (Fig. 2), we find that ~~the~~ CO_2 ~~flux exhibits a~~ fluxes exhibit high temporal variability between positive and negative CO_2 fluxes from most wind directions. In the wind sector between 60°~~– 120~~–120°, the flux source area is dominated by the merged polygonal pond. The CO_2-C fluxes from this pond sector show ~~a smaller variability (mean of 0.06~~ smaller absolute variability ($0.09\ ^{0.38}_{-0.33}$ g m^{-2} d^{-1}~~with a standard deviation of 0.28 g m^{-2} d^{-1}~~, Median $^{95\ \%\ \text{Percentile}}_{5\ \%\ \text{Percentile}}$) than the fluxes from all other wind directions (~~mean of -0.17~~ $-0.08\ ^{0.87}_{-1.56}$ g m^{-2} d^{-1}~~with a standard deviation of 0.77 g m^{-2} d^{-1}~~, Median $^{95\ \%\ \text{Percentile}}_{5\ \%\ \text{Percentile}}$). Additionally, we observe a lower respiration rate from the merged polygonal pond than from the semi-terrestrial tundra. Fig. 3 shows the observed night-time CO_2 fluxes plotted against the respective weighted footprint fraction of open water. We define nighttime as PAR<20 µmol m^{-2} s^{-1}~~and expect only respiration and no photosynthesisduring these times~~; we expect that there would only be respiration, no photosynthesis, during the night-times. We find that the fluxes decrease ~~with an increasing open-water contribution~~ as the pond area contribution increases. Thus, the strength of CO_2 respiration shows a dependence on the ~~open-water contribution~~ contribution of open-water. We also find that low air temperatures are mostly associated with low respiration rates.

Another ~~part of the~~ aspect of CO_2 flux variability stems from the diurnal cycle. We compare the diurnal cycle of the CO_2 fluxes from the merged polygonal pond (estimated ~~following equation~~ in accordance with Eq. 4) and the semi-terrestrial tundra (Eq. 5, Fig. 4)~~, and we see~~ . The results show a less pronounced diurnal CO_2 cycle from the direction of the merged polygonal pond (blue) compared to the diurnal CO_2 cycle from the semi-terrestrial tundra (green). ~~All~~ We combine all data from the merged polygonal pond ~~combined~~ (F_{pond} in Eq. 4)~~result~~ , which results in a CO_2-C flux of $\mathbf{0.13}\ ^{\mathbf{0.24}}_{\mathbf{0.00}}$ g m^{-2} d^{-1} (~~Median~~ $^{75\%\ \text{Percentile}}_{25\%\ \text{Percentile}}$Median $^{75\ \%\ \text{Percentile}}_{25\ \%\ \text{Percentile}}$).

3.3 CH_4 fluxes

~~When plotting~~ We plot the observed CH_4 fluxes against wind direction (Fig. 5)~~, we see~~ . The results show that the CH_4 emissions peak at $\sim 120°$, where fluxes from one shoreline of the merged polygonal pond contribute to the observed flux (Fig. 1 d, from now on $shore_{120°}$). We do not observe a similar peak of CH_4 emissions in the direction of the second shoreline towards $\sim 50°$ ($shore_{50°}$). These peaks did not correlate with ~~any of the four~~ a specifically large contribution of one of the land-cover classes to the footprint.

To further investigate the peak at $shore_{120°}$, we compare the CH_4 emissions from the different wind sectors ($shore_{120°}$, $shore_{50°}$, *pond* and *tundra*, ~~section~~ Sect. 2.4.5). We find the following fluxes from the wind sectors: $19.18\ ^{24.47}_{14.26}$ mg m^{-2} d^{-1} ($shore_{120°}$), $12.96\ ^{15.11}_{10.34}$ mg m^{-2} d^{-1} ($shore_{50°}$), $13.90\ ^{18.46}_{11.02}$ mg m^{-2} d^{-1} (*pond*), and $12.55\ ^{16.07}_{9.65}$ mg m^{-2} d^{-1} (*tundra*, ~~*Median*~~ $^{75\%\ \textit{Percentile}}_{25\%\ \textit{Percentile}}$Median $^{75\ \%\ \text{Percentile}}_{25\ \%\ \text{Percentile}}$). Fluxes from $shore_{120°}$ have a higher median than fluxes from the other three wind sectors (Fig. 6).

We investigated the impact of wind speed and air temperature on the CH_4 fluxes by excluding flux intervals with high wind speed (~~larger~~ greater than 5 m s^{-1}) and high air temperature (~~larger~~ warmer than 12 °C). ~~In the~~ The randomization test (~~section 2.4.6) , we find evidence for~~ Sect. 2.4.6) provided evidence of a significant difference between ~~the~~ CH_4 ~~emission~~ emissions

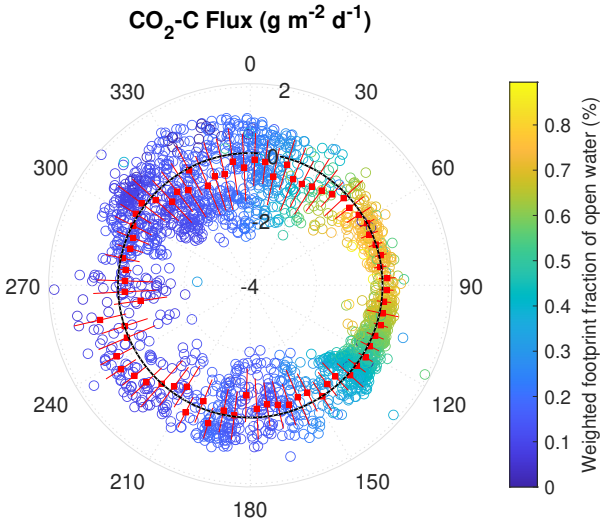

Figure 2. Polar plot of observed ~~30-min~~ 30-minute CO_2-C ~~flux~~ fluxes with respect to the wind direction~~at the EC tower~~. Negative values (inside of the ~~dotted~~ solid black line) represent CO_2 uptake, while positive values (outside of the dotted black line) represent CO_2 ~~emission~~emissions. The values -4, -2, 0, and 2 indicate the magnitude of the CO_2-C flux in g m^{-2} d^{-1}. The color of each point on the plot represents the percentage the point comprises of the total open water weighted footprint fraction in each 30-minute flux. The red boxes indicate the mean CO_2 flux of 5~~°~~° wind direction intervals during the ~~2-months~~ two-month observation period (red lines indicate the first standard deviation).

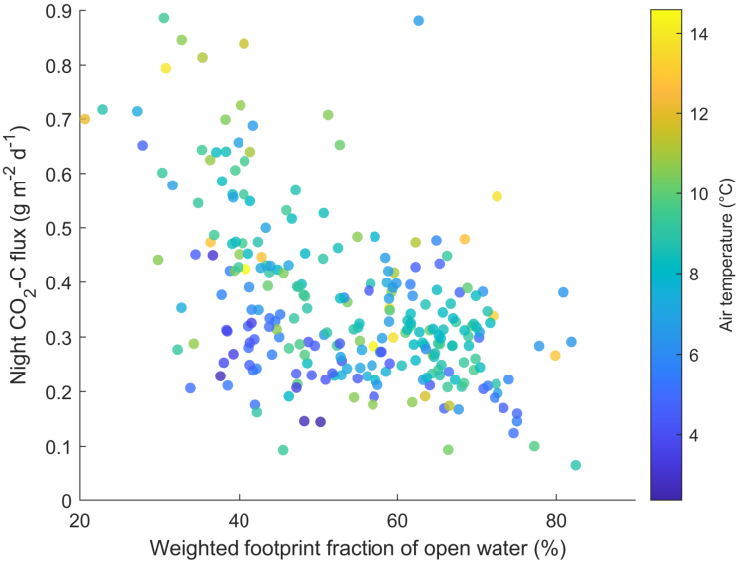

Figure 3. Scatter plot of observed CO_2 fluxes against the weighted footprint fraction of open water ~~in~~ during each 30-minute flux~~with~~. The air temperature ~~as~~ is represented through color. Only fluxes observed at nighttime (PAR<20 µmol m^{-2} s^{-1}) are shown.

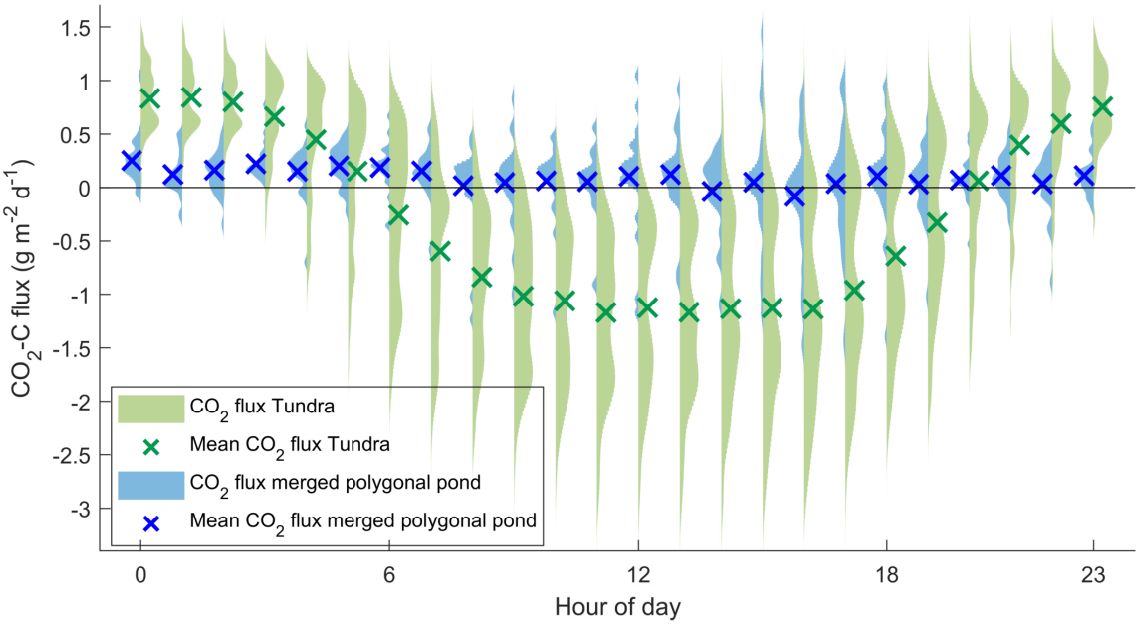

Figure 4. Diurnal cycle of modeled CO_2-C based on observations flux from the merged polygonal pond (blue, eq. 4) and the semi-terrestrial tundra (green, eq. 5) as violin plots for each half-hour flux. Blue and green crosses mark the mean CO_2-C flux during each half-hour flux. A violin plot shows the distribution of measurements along the y-axis – the width of the curves ~~expresses the density of data points at each~~ indicates how frequently a certain y-value occurred.

from *shore*$_{120°}$ and the other three wind sector classes at low wind speeds (top row in Fig. A4) and no significant difference between the CH_4 emission from the classes *pond* - *tundra* and *shore*$_{50°}$ - *tundra*. The difference between the classes *pond* and *shore*$_{50°}$ is significant~~, however~~; however, it is much smaller than the previously described differences (see center graph in Fig. A4). Note that the CH_4 emissions from ~~the pond and the tundra~~ *pond* and *tundra* have a similar magnitude under moderate wind speed conditions. The results are very similar for moderate temperatures: We find evidence ~~for~~ of a significant difference between the CH_4 ~~emission~~ emissions from *shore*$_{120°}$ ~~to the other three~~ and the CH_4 emissions from the other three wind sector classes (top row in Fig. A5). The differences in medians between the *pond* and *shore*$_{50°}$ and between the *pond* and *tundra* are significant. However, this difference is much smaller (second row in Fig. A5). In summary, ~~we find that~~ neither high wind speed nor high temperatures act as a driver for the high CH_4 emission from *shore*$_{120°}$. In contrast, the peak at $180° - -190°$ can be explained reasonably well using air temperature and friction velocity in a multiple linear regression ($R^2 = 0.44$). Using the same predictors results in an R^2 of 0.20 for the peak at *shore*$_{120°}$.

The ratio of CO_2-C to CH_4-C emissions at night (PAR<20 µmol m^{-2} s^{-1}) has a value of $CH_4/CO_2 = 0.060^{0.076}_{0.049}$ for fluxes with an open-water weighted footprint fraction of more than 60 %, whereas the ratio amounts to ~~(~~$CH_4/CO_2 = 0.020^{0.024}_{0.015}$ ~~,~~ ~~Median$^{75\%\ \text{Percentile}}_{25\%\ \text{Percentile}}$~~(Median $^{75\ \%\ \text{Percentile}}_{25\ \%\ \text{Percentile}}$) for fluxes with an open-water weighted footprint fraction of less than 20 %.

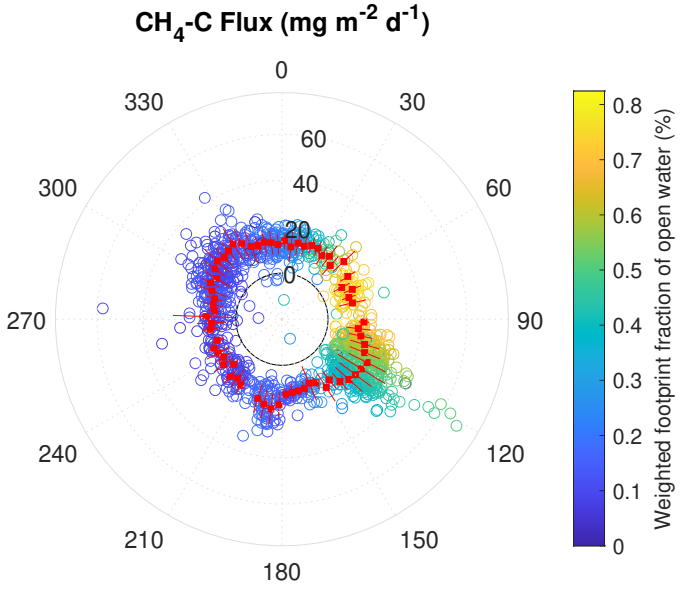

Figure 5. Polar plot of 30-minute observed CH_4-C flux with respect to the wind direction at the EC tower. Positive values outside the ~~dotted~~ solid black line represent CH_4 ~~emission~~emissions, while values and inside the line ~~,~~ represent CH_4 uptake during one half-hour period. The values 0, 20, 40, and 60 indicate the magnitude of the CH_4-C flux in mg m^{-2} d^{-1}. The color of each point on the plot represents the percentage the point comprises of the total open water weighted footprint fraction in each 30-minute flux. The red boxes indicate the mean CH_4 flux of 5~~°~~° wind direction intervals during the ~~2-months~~ two-months observation period (red lines indicate the first standard deviation).

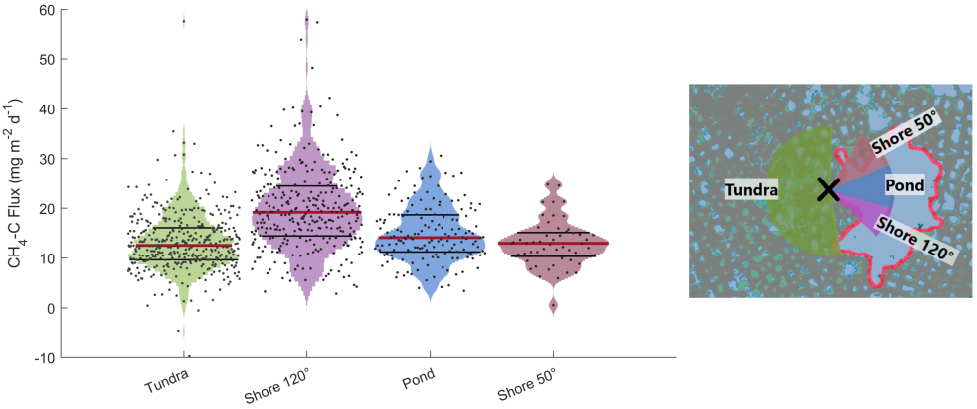

Figure 6. Violin plots of observed CH_4 emissions at the EC tower separated into four different wind ~~direction~~ sector classes. A violin plot shows the distribution of measurements along the y-axis - the width of the curves ~~expresses the density of data points at each~~ indicates how frequently a certain y-value occurred. Medians of CH_4 emission distributions are shown as red lines, and 75th ~~&~~ and 25th percentile are shown as black lines. On the right, the wind sectors with the eddy covariance tower in the center (black cross) are shown.

3.4 Upscaled CO_2 flux

We use the estimated open-water CO_2 flux from the merged polygonal pond and the modeled CO_2 flux from the semi-terrestrial tundra to linearly up-scale the CO_2 flux for the polygonal tundra of Samoylov Island (excluding larger ~~thermokarst~~ lakes, the method described in ~~section~~ Sect. 2.4.4). As we have ~~no~~ not obtained estimates for the CH_4 fluxes from ~~the landcover types~~ *tundra* and *pond* land-cover types, we only upscale CO_2.

We estimate that ~~the landscape~~ when one includes the CO_2 ~~uptake is ~ 11% lower when including the~~ flux from thermokarst ponds, the river terrace landscape's CO_2 ~~flux from ponds compared to a~~ uptake is ~ 11% lower than the uptake of semi-terrestrial tundra without ponds. The modeled CO_2-C flux from the semi-terrestrial tundra (without consideration of thermokarst pond fluxes) accumulated to -16.29 $\pm$ 0.43 g m^{-2} during the observation period (60.5 days). ~~Separated~~ If separated into months, ~~it~~ the modeled CO_2-C flux from the semi-terrestrial tundra amounts to -15.01 $\pm$ 0.26, -3.56 $\pm$ 0.33 and +2.35 $\pm$ 0.11 g m^{-2} in July (19.8 days), August (31 days), and September (9.7 days), respectively. When ~~including~~ one includes the CO_2 flux from the merged polygonal pond ~~as representative for all~~ to represent all thermokarst ponds on Samoylov ~~island~~Island, the resulting estimate of the landscape CO_2 flux amounts to -14.47 $\pm$ 0.40 g m^{-2} (60.5 days)~~and~~ , with monthly fluxes of -13.75 $\pm$ 0.24, -2.99 $\pm$ 0.31, and +2.27 $\pm$ 0.10 g m^{-2} in July (19.8 days), August (31 days), and September (9.7 days), respectively. Thus, the results show that thermokarst ponds have the largest impact on the landscape's CO_2 flux in August. In September, accounting for thermokarst ponds leads to a 3.5 % lower ~~landscape~~ estimate of landscape CO_2 emissions.

4 Discussion

4.1 CO_2 flux

Only a limited number of EC CO_2-flux studies from permafrost-affected ponds and lakes are available (studies with "EC" in Tab. 1). Estimates of open-water EC CO_2-C flux range from 0.059 g m^{-2} d^{-1} (Jammet et al., 2017)~~over~~ , to 0.11 g m^{-2} d^{-1} (Eugster et al., 2003), to 0.22 g m^{-2} d^{-1} (Jonsson et al., 2008). Our estimate of $0.12\ ^{0.24}_{0.0014}$ g m^{-2} d^{-1} is, therefore, well within the range of open-water CO_2-C fluxes observed with the EC method. Other studies using different methods report a wider range of open-water CO_2 fluxes in arctic regions. These fluxes range from a minor CO_2-C uptake (-0.14 g m^{-2} d^{-1}, Bouchard et al. (2015)) to substantial emissions of CO_2-C (up to 2.2 g m^{-2} d^{-1}, Abnizova et al. (2012)). A modeling study involving multiple lakes in ~~north-eastern~~ Northeast European Russia found ~~close to~~ that they produce almost zero emissions (0.028 g m^{-2} d^{-1}, Treat et al. (2018)). ~~Our perhaps most striking finding is that~~

Strikingly, our estimates of open-water CO_2 emissions are ~~approx. 12-18~~ approximately 12–18 times smaller than those that have been previously reported for open-water CO_2 emissions at the same study site (Abnizova et al., 2012). One reason for the divergent results might be the different methods used. In Abnizova et al. (2012), the thin boundary layer model (TBL)~~after Liss and Slater (1974)~~, following Liss and Slater (1974), was applied to estimate CO_2 emissions from CO_2 concentrations~~measured in water samples~~. However, one other study found good agreement between the EC method and the TBL (Eugster et al., 2003). ~~Abnizova et al. (2012) measured smaller thermokarst ponds, as opposed~~ In addition, in contrast to the larger

Table 1. Daily mean water-atmosphere CO_2 & CH_4 fluxes from different study sites. TBL is the abbreviation for thin boundary layer model, EC for eddy covariance, CH for chamber measurement, MOD for modelled fluxes, STO for storage fluxes, and NEW for the method used in this study. All fluxes are given ± standard deviation, except of fluxes from this study are given as Median $^{75\%\ \text{Percentile}}_{25\%\ \text{Percentile}}$.

Study	Location	Period/Time	Study Site	Method	CO_2-C flux ($g\ m^{-2}\ d^{-1}$)	CH_4-C flux ($mg\ m^{-2}\ d^{-1}$)
This study	Lena Delta, Northern Siberia	11.07.– 10.09.2019	merged polygonal pond	EC/NEW	$0.13\ ^{0.24}_{0.00}$	$14.10\ ^{18.67}_{11.23}$
			merged polygonal pond shore	EC	–	$12.96\ ^{15.11}_{10.34} - 19.18\ ^{24.47}_{14.26}$
Abnizova et al. (2012)	Lena Delta, Northern Siberia	01.08. – 21.09.2008	Samoylov Pond	TBL	1.50 – 2.20	–
			Samoylov Lake	TBL	1.40 – 2.10	–
Jammet et al. (2017)	Northern Sweden	2012 – 2013	Lake Villasjön	EC	0.059	13.42 ± 1.64
Jonsson et al. (2008)	Northern Sweden	17.06. – 15.10.2005	Lake Merasjärvi	EC	0.22 ± 0.002	–
				TBL	0.30 ± 0.01	
Eugster et al. (2003)	Alaska	27.07 – 31.07.1995	Toolik Lake	EC	0.11 ± 0.033	–
				TBL	0.13 ± 0.003	
				CH	0.37 ± 0.060	
Jansen et al. (2019)	Northern Sweden	Year round, 2010 – 2017	Villasjön	CH	0.22 ± 0.047	14.04 ± 2.25
			Inre Harrsjön		0.25 ± 0.05	10.39 ± 1.40
			Mellersta Harrsjön		0.73 ± 0.067	13.76 ± 2.81
Bouchard et al. (2015)	NE Canada	July 2013 & 2014	Bylot Island, Polygon ponds	TBL	-0.14 – 0.74	0.50 – 6432
			Lakes		-0.085 – 0.062	0.70 – 74.5
Sepulveda-Jauregui et al. (2015)	Alaska	June – July 2011 & 2012	8 Lakes, Yedoma	TBL & STO	0.60 ± 0.58	92.86 ± 35.72
			32 Lakes, Non-Yedoma		0.10 ± 0.10	16.80 ± 8.61
Treat et al. (2018)	Northeast European Russia	2006 – 2015	Multiple Lakes	MOD	0.028 ± 0.00011	0.84 ± 0.0
Sieczko et al. (2020)	Northern Sweden	July – August 2017	Lake Ljusvatterntjärn	CH	–	2.95 ± 0.75
Ducharme-Riel et al. (2015)	North-East Canada	Summer 2008	15 lakes	TBL	0.20 ± 0.093	–
Repo et al. (2007)	Western Siberia	03.07. – 06.09.2005	MTlake	TBL	0.14 ± 0.11	–
			FTlake	TBL	0.41 ± 0.25	
			MTpond	TBL	0.44 ± 0.25	
Lundin et al. (2013)	Northern Sweden	2009 (only ice-free season)	27 lakes	TBL	0.18 ± 0.11	–
Kling et al. (1992)	Alaska	1975 – 1989	25 lakes	TBL	0.25 ± 0.040	5.16 ± 0.96

merged polygonal pond we focus on. While this might explain the deviations, there are also thermokarst ponds highly similar to the ones in Abnizova et al. (2012) in the footprint of the EC tower in this study . If those ponds , Abnizova et al. (2012) measured two polygonal ponds (they took 46 water samples in August and September 2008). These two ponds might have had exceptionally high CO_2 concentrations and might not be representative of polygonal ponds in our study area. If the polygonal ponds in the footprint of our EC measurements emitted CO_2 in the quantities suggested by Abnizova et al. (2012), we would expect to see their signal more clearly in our measurements. Thus, we cannot conclusively resolve the differences.

Our approach of combining a footprint model with a land-cover classification to extract fluxes from different land-cover classes allows us to determine the thermokarst pond CO_2 flux. We report an uncertainty range of the in respect of the thermokarst pond CO_2 flux; however, we cannot identify identifying the full uncertainty of this flux in is not possible using this approach due to the unknown uncertainty of the footprint analysisfootprint analysis' unknown degree of uncertainty. Still, the results in respect of the thermokarst pond CO_2 flux results are plausible and in the correct expected order of magnitude for two reasons. First, a reduced diurnal variability has been is observed when the merged polygonal pond influences the flux signal (Fig. 4). This reduction indicates that the respiration rate from the merged polygonal pond is lower than the respiration rate from the semi-terrestrial tundra, where ample oxygen is available in the upper soil layer. Additionally, there is less photosynthesis since the since the thermokarst ponds have a lower vegetation density than the tundra, there is less photosynthesis. Second, when focusing on night-time fluxes, when only respiration occurs , and (i.e. no carbon is taken up), there is a decrease in CO_2 emission emissions with an increasing weighted footprint fraction of open water (Fig. 3), also indicating ; this also indicates that there was reduced decomposition in the merged polygonal pond. Overall, the lower emissions from the pond compared to the based on the data, the findings that thermokarst ponds have lower CO_2 emissions than the semi-terrestrial tundra are reasonable.

4.2 CH_4 flux

We observe large differences in CH_4 emission from different emissions from the four wind sectors. CH_4 emissions from $shore_{120°}$ are significantly higher than from $shore_{50°}$, *pond*or , and *tundra* (section Sect. 3.3). Notably, we tested the dependence of these higher fluxes on wind speed and air temperature. We expect high wind speeds to enhance turbulent mixing of the water column and diffusive CH_4 outgassing at the water-atmosphere interface. High wind speeds are also associated with pressure pumping, which potentially fosters the ebullition of CH_4. On the other hand, peak temperatures can lead to peak CH_4 production and emissions due to enhanced biological activity. However, the high emissions from $shore_{120°}$ do not coincide with meteorological conditions of either of two key meteorological conditions, high wind speeds or and high temperatures, which would especially favor high emissions. Thus, the difference in methane flux dynamics between $shore_{120°}$ and $shore_{50°}$ is astounding since the shorelines share many characteristics. Both other characteristics.

Both shorelines extend radially (in a fairly straight line) from the EC tower (Fig. 1), thus contributing similarly to the EC flux. The underwater topography does not vary much significantly between the two shorelines. Both Meters away from the shore, both shorelines have a water depth between of a few centimeters and a few decimeters within meters away from the shore (see data from Boike et al. (2015a)). As previously described in section 2.1, both shorelines are dominated by *Carex aquatilis*, and

from visual inspection, we ~~cannot find~~ could not identify differences in shoot density. We, therefore, assume that the ~~vegetation type does~~ characteristics of the emergent vegetation do not play a major role in explaining the differences between the CH_4 ~~emission~~ emissions from $shore_{120°}$ and $shore_{50°}$. We also examine the evolution of the shorelines at the merged polygonal pond to check whether erosion along the shoreline could ~~drive~~ cause the high CH_4 emissions. We compare ~~a coarse~~ an image from 1965 (U.S. Geological Survey, EROS Center, 1965) with the current (2019) shoreline, yet we cannot identify signs of recent erosion. ~~Also~~Furthermore, high-resolution aerial images of ~~the~~ this pond from 2008 (Boike et al. (2015b), resolution $>$ 0.33 m) and 2015 (Boike et al. (2015c), resolution $>$ 0.33 m) show no signs of erosion. ~~Thus, we exclude erosion as a driving factor of high~~ We therefore assume that past erosion is unlikely is unlikely to have been a factor that caused the high levels of CH_4 emissions ~~.~~ we observed in 2019.

~~We also consider the possibility that local~~ Local ebullition of the merged polygonal pond could lead to high CH_4 emissions from $shore_{120°}$. We ~~apply~~ applied the method proposed by Iwata et al. (2018) to check for signs of ebullition events. This method uses the 20 Hz raw ~~concentration of~~ CH_4 concentration data to detect short-term peaks in CH_4 that originate from ebullition events. However, we cannot detect ebullition events in the 20 Hz raw data.

In summary, ~~many causes, such as~~ meteorological conditions (wind speed ~~or~~ and temperature), ~~vegetation type~~characteristics of emergent vegetation, coastal erosion, and intense ebullition events, ~~can be excluded as driving factors . Therefore, the most likely cause of the~~ are unlikely to be the main driving factors of the increased CH_4 emissions we observed. Another possible driver of higher CH_4 emissions from $shore_{120°}$ ~~might be~~ is a small but steady seep ebullition hot spot close to this shoreline (such as ebullition class *Kotenok* in Walter et al. (2006)). Seep ebullition hot spots have been reported to occur heterogeneously in clusters in Alaskan lakes (Walter Anthony and Anthony, 2013). ~~So, a future~~ Unfortunately, seep ebullition has not previously been reported in water bodies in our study area, so we did not include measurements targeting this process in our measurement campaign. In future studies, visual inspection of trapped CH_4 bubbles in the ice column during wintertime, as proposed ~~in~~ by Vonk et al. (2015), could reveal more information about the cause of the higher CH_4 ~~emission from the~~ emissions from $shore_{120°}$, as could funnel or chamber measurements with high spatial coverage.

The results show that the merged polygonal pond emits ~~CH_4 with~~ a similar magnitude ~~as the~~ of CH_4 as the polygonal tundra surface under similar meteorological conditions and when excluding the high emissions from $shore_{120°}$. However, substrate availability and temperature dynamics differ substantially. Additionally, in dense soils, methane diffuses ~~through upper soil layers and can oxidize~~ slowly enough through soil layers containing oxygen that the methane can be oxidized before reaching the surface. In contrast, methane emitted in ponds can reach the surface quickly through ebullition or ~~higher~~ plant-mediated transport in addition to diffusion. Therefore, we expect ~~bigger differences between~~ to see larger differences between the CH_4 emissions from the merged polygonal pond and the polygonal tundra, more ~~like the differences~~ akin to the differences that have been detected in a subarctic lake and fen ~~(Jammet et al., 2017). Yet~~by Jammet et al. (2017). However, we see no significant difference in the CH_4 ~~emission~~ emissions from the open-water areas of the merged polygonal pond and the polygonal tundra surface (Fig. 6 & A4).

Since many other ~~ponds~~ thermokarst ponds in our study area are smaller than the merged polygonal pond (making them unsuitable ~~for studying with~~ to study using the EC method), and since smaller ponds tend to be ~~stronger emitters~~ greater

emitters of methane (Holgerson and Raymond, 2016; Wik et al., 2016), our measurements might provide a lower limit of overall ~~pond-CH~~thermokarst pond CH_4 emissions.

We estimate a CH_4-C flux of 13.38 $^{15.92}_{10.55}$ mg m^{-2} d^{-1} (~~*Median* $^{75\%Percentile}_{25\%Percentile}$~~Median $^{75\ \%\ \text{Percentile}}_{25\ \%\ \text{Percentile}}$) from the merged polygonal pond and 12.96 $^{15.11}_{10.34}$–19.18 $^{24.47}_{14.26}$ mg m^{-2} d^{-1} from the shores of this pond. This is higher than the fluxes measured by Jammet et al. (2017) from a sub-arctic lake (Tab. 1). The authors report a mean annual CH_4-C flux of 13.42 $\pm$ 1.64 mg m^{-2} d^{-1} and a mean ice-free season CH_4-C flux of 7.58 $\pm$ 0.69 mg m^{-2} d^{-1}. A study focusing on 32 non-Yedoma thermokarst lakes in Alaska found CH_4-C emissions similar to our results (16.80 $\pm$ 8.61 mg m^{-2} d^{-1}, Sepulveda-Jauregui et al. (2015)). Also, a synthesis of 149 thermokarst water bodies north of $\sim 50°$ reports CH_4-C emissions in the same order of magnitude (27.57 $\pm$ 14.77 mg m^{-2} d^{-1}, Wik et al. (2016)). However, ~~there is also a recent study reporting~~ other recent studies have reported considerably lower CH_4-C emissions of 2.95 $\pm$ 0.75 mg m^{-2} d^{-1} in Northern Sweden (Sieczko et al., 2020) and, in contrast, a study finding CH_4-C emissions of up to ~~6432~~ 6,432 mg m^{-2} d^{-1} in ~~North-East~~ Northeast Canada (Bouchard et al., 2015). The wide range of water-body methane emissions ~~cautions us to be careful~~ militates in favor of caution when generalizing our results, even for Samoylov Island, especially since the emissions within the ~~pond are already~~ merged polygonal pond have been shown to be heterogeneous. Instead, after finding a hotspot in CH_4 emission at the pond shore, we would like to highlight ~~the need for spatially representative observation and mapping of~~ that the gathering of additional measurements – for example employing funnel traps or counting bubbles in ice – will help to better constrain thermokarst pond CH_4 ~~fluxes to understand the variability of pond-CH~~dynamics in their full complexity. Nevertheless, our measurements provide a robust lower limit of thermokarst pond CH_4 emissions~~better.~~.

4.3 Upscaling the CO_2 flux

We upscale the CO_2 emissions for the river terrace ~~of Samoylov, the area where~~ on Samoylov, an area for which we have access to ~~the~~ a high-resolution land-cover classification. We find that ~~not accounting for pond-CO_2 emission leads to an overestimating the polygonal tundra landscape's sink function~~ we overestimate the carbon-dioxide uptake of the polygonal tundra by 11 % when we do not account for the thermokarst ponds' CO_2 emissions. A similar approach by Abnizova et al. (2012) found a potential increase of ~~35 – 62~~ 35–62 % in the estimate of CO_2 emission from the Lena River Delta when including small ponds and lakes ~~into~~ in the landscape CO_2 emission calculation. If we follow the upscaling approach by Abnizova et al. (2012) and consider overgrown water as part of the ~~ponds, we even find a~~ thermokarst ponds, the estimate of the landscape CO_2 ~~emission reduction of~~ uptake would decrease by 19 %. Kuhn et al. (2018) also found water bodies in arctic regions to be an important source of carbon, which could outbalance the ~~tundra's sink function~~ carbon dioxide uptake of the semi-terrestrial tundra in a future climate. In summary, our results demonstrate that open-water CO_2 emissions can substantially influence the summer carbon balance of the polygonal tundra~~during the growing season. When looking at the night-time~~. With respect to the night time emissions, we find that per gram CO_2-C thermokarst ponds emit 0.06 g CH_4-C ~~are emitted from ponds and only~~ whereas the semi-terrestrial tundra only emits 0.02 g CH_4-C~~from the semi-terrestrial tundra~~. This finding underlines again ~~, that~~that, especially when considering thermokarst ponds, CH_4 emissions are of ~~high~~ significant interest. Even though mean CH_4 emissions from the semi-terrestrial tundra and open water are of similar magnitude, we expect that the impact

of thermokarst ponds on the carbon balance would be even ~~bigger~~ greater when accounting for CH_4 due to ~~the~~ locally high emissions.

Our results ~~indicate~~ suggest that future studies ~~aiming~~ that aim to capture a representative landscape flux should pay extra attention to the water bodies in their footprint. The CO_2 flux from thermokarst ponds has the opposite sign ~~to the tundra~~(CO_2 emission) as the semi-terrestrial tundra (CO_2 uptake) during the observation period. Consequently, thermokarst ponds should cover about as much area in the ~~footprint~~ measurement as they do in the landscape area of interest. In this way, the chances of capturing CH_4 hotspots~~are also higher~~, which can ~~then~~ be investigated more closely, are also greater.

5 Conclusions

We find that thermokarst ponds are a carbon source. At the same time, the surrounding ~~tundra is~~ semi-terrestrial tundra in our study area acts as a carbon sink during the ~~period July – September~~ summer period (July–September), which is in agreement with prior studies (Abnizova et al., 2012; Jammet et al., 2017), ~~even if~~ despite that we observe much lower open-water CO_2 fluxes compared to previous work at the same study site (Abnizova et al., 2012). Using our approach to disentangle the EC fluxes from different ~~land cover~~ land-cover classes, we ~~gauge~~ posit that during the measurement period, ~~not accounting for ponds leads to overestimating the landscape CO_2 sink~~ we would overestimate the carbon-dioxide uptake of the polygonal tundra by 11 ~~%~~% if we had not accounted for thermokarst ponds. We expect lakes to have a similar effect on the carbon budget, though a smaller one, since lakes (a) cover a similar ~~area as~~ amount of surface area as the thermokarst ponds in our study site (Abnizova et al., 2012; Muster et al., 2012) and (b) are weaker emitters of greenhouse gases than ponds (Holgerson and Raymond, 2016; Wik et al., 2016).

In contrast to ~~the spatially more homogeneous~~ CO_2 emissions, which are spatially more homogeneous, small-scale heterogeneity in CH_4 emissions makes it difficult to find drivers of CH_4 emissions. We cannot pinpoint the drivers behind the high emissions ~~at~~ along parts of the coastline, which we surmise were potentially caused by seep ebullition. Thus, we cannot estimate the impact of this heterogeneity on the landscape scale and, therefore, refrain from upscaling CH_4 emissions. Additionally, the open-water fluxes presented in this paper originate from a single merged polygonal pond since the other polygonal ponds surrounding the EC tower are too small to extract their fluxes ~~with~~ using the footprint method applied here. ~~So~~Thus, we do not account for the spatial variability of CH_4 emissions between thermokarst ponds, which can be substantial (Rehder et al., 2021; Wik et al., 2016). However, we note that open-water fluxes were of a similar magnitude as the polygonal tundra fluxes. Consequently, the main impact ~~of ponds~~ that thermokarst ponds have on the landscape CH_4 budget might ~~be~~ occur through plant-mediated transport and local ebullition.

While being ill-suited for the study of smaller ponds, we ~~want to~~ underline that the EC method is appropriate for observing greenhouse-gas fluxes from ~~ponds with an area~~ thermokarst ponds as small as $0.024\ km^2$. The EC method has a higher temporal resolution than the TBL method. It does not disturb ~~the~~ exchange processes like the ~~chamber-flux method, eliminating~~ chamber flux method, which eliminates the wind at the water surface. Especially when combining ~~the~~ an EC footprint with a ~~land cover~~

~~classification, we can distinguish~~ land-cover classification, one can distinguish between the contribution of different ~~land cover classes well and~~ land-cover classes effectively and also study the fluxes from thermokarst ponds.

We conclude that thermokarst ponds contribute significantly to the landscape carbon budget. Changes in ~~the Arctic~~ arctic hydrology and the concomitant changes in the water-body distribution ~~may impact the overall carbon budget of the Arctic and flip a landscape from being an overall carbon sink to becoming an overall carbon source~~in permafrost landscapes may cause these landscapes to change from being overall carbon sinks to overall carbon sources.

Code and data availability. The data has been published at Pangaea (https://doi.org/10.1594/PANGAEA.937594). Code can be requested from the authors.

Appendix A: Additional figures

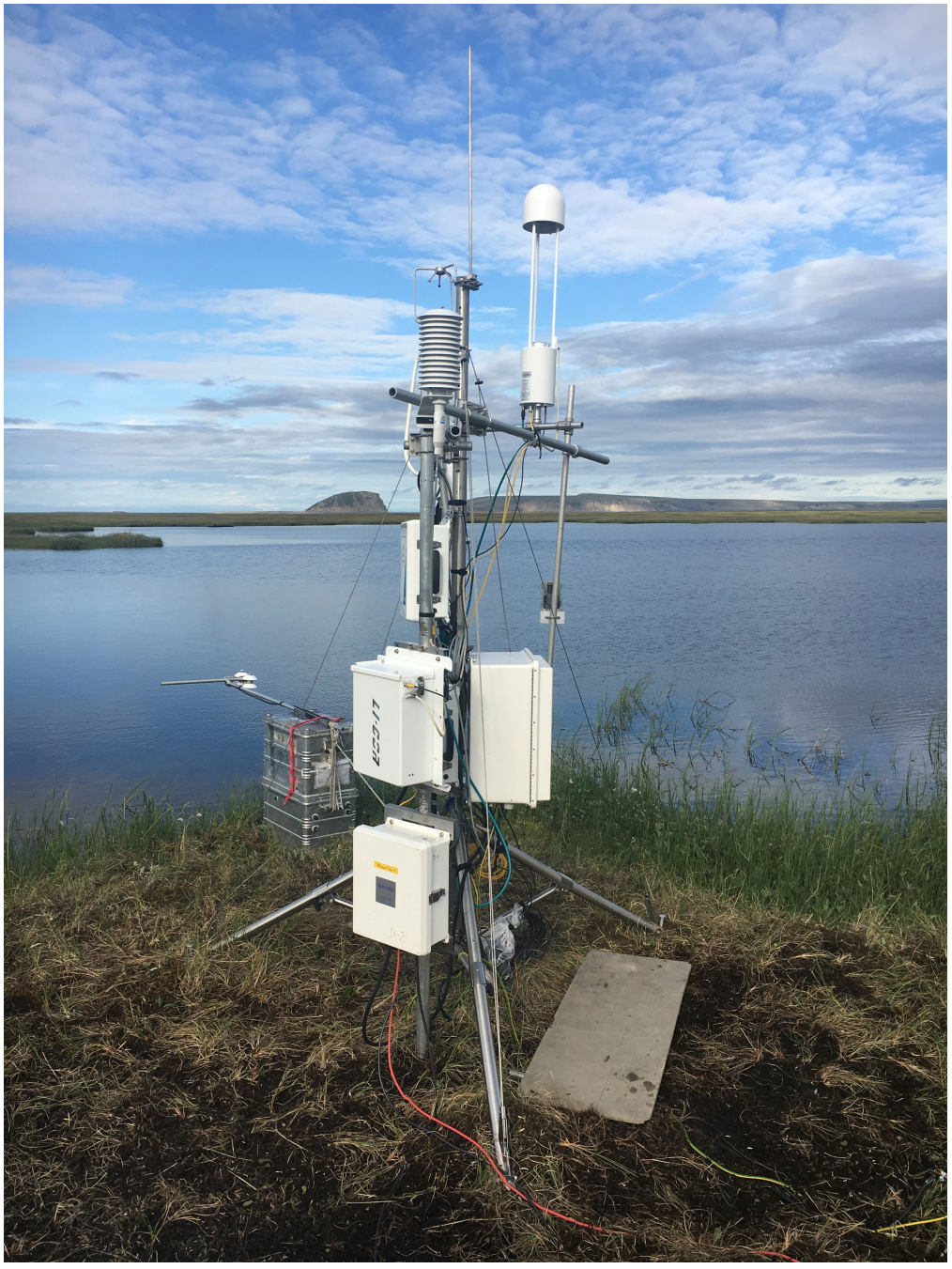

Figure A1. Picture of the eddy covariance tower with the merged polygonal pond in the background. Picture taken on 11 July 2019 by Zoé Rehder.

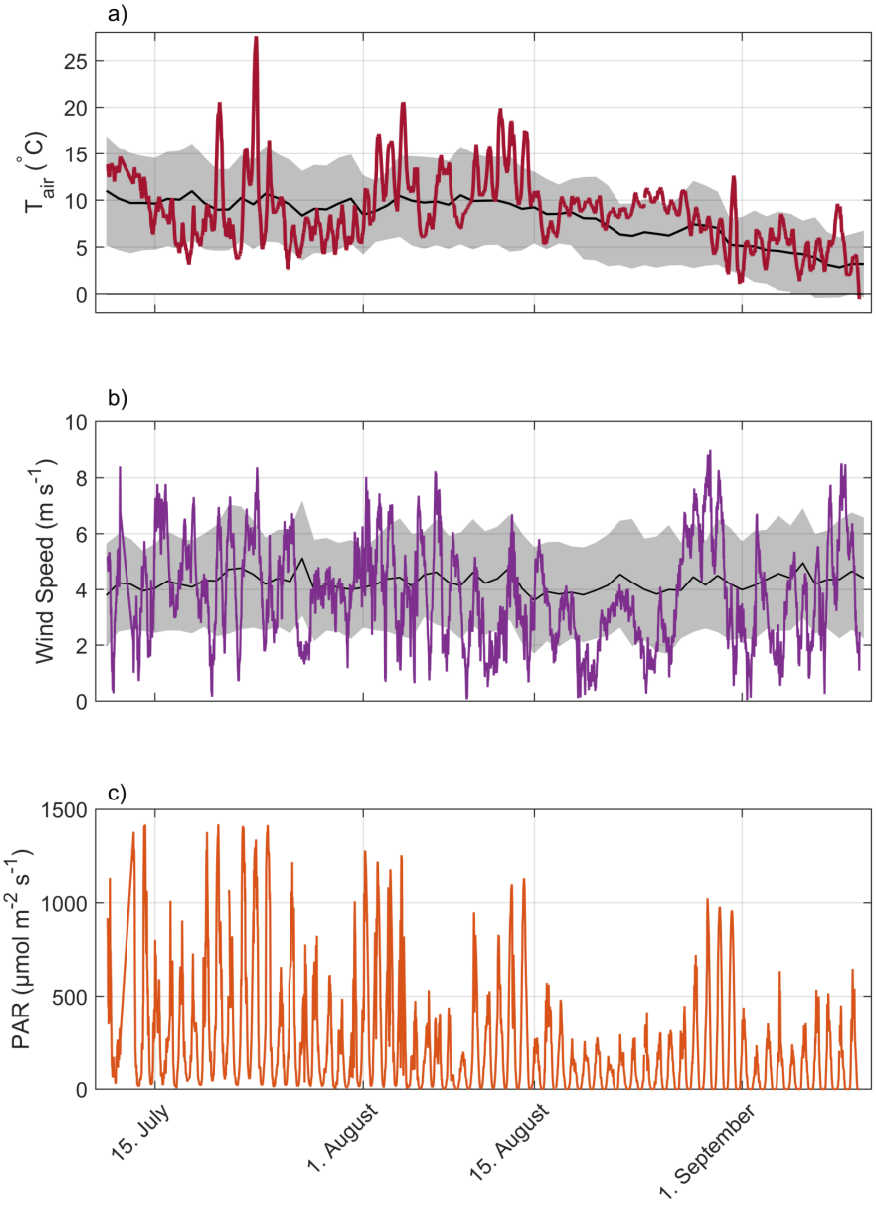

Figure A2. Timeline of observed meteorological conditions during the observation period with air temperature in 2 meters height (a), wind speed in 3 meters height (b) and photosynthetically active radiation (PAR) (c). Mean values and standard deviation of observations during the past 16 years are plotted as black lines and gray areas.

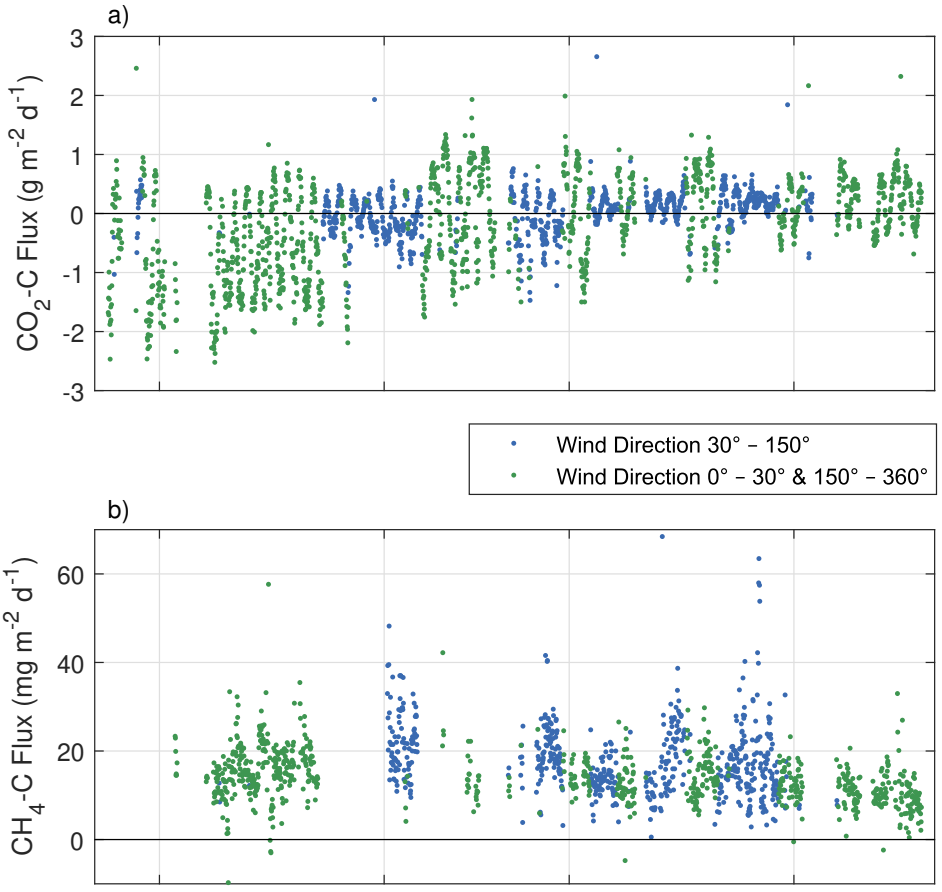

Figure A3. Time series of 30-minute observed CO_2-C flux intervals (a) and CH_4-C flux with a quality flag of 0 or 1. The blue color represents fluxes originating from the wind direction of the ~~lake~~ merged polygonal pond ($30° - 150°$ wind direction, mostly mixed signals from semi-terrestrial tundra and the ~~lake~~ surface of the merged polygonal pond) and the green color represents fluxes originating from all other wind directions.

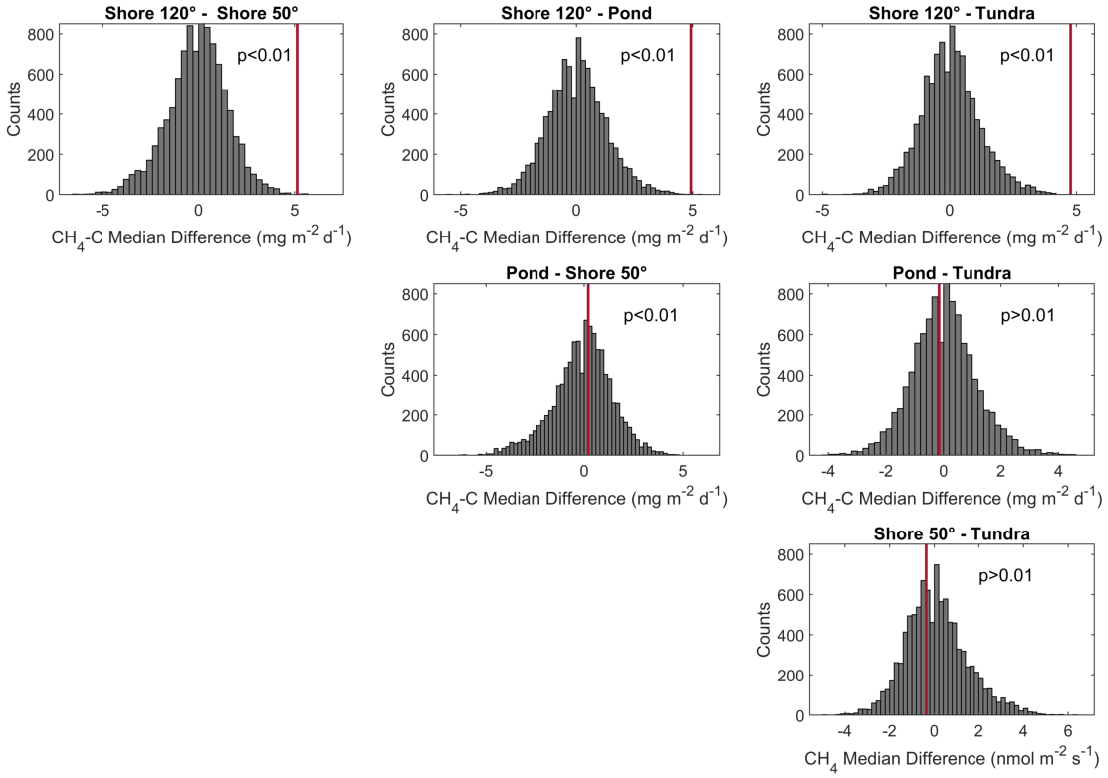

Figure A4. Histogram of permutation tests between the medians of CH_4 emissions from different wind direction classes in figure 6. All medians from flux observations during moderate wind speed conditions. The observed differences in medians between the different wind direction classes are shown in red vertical bars in each plot.

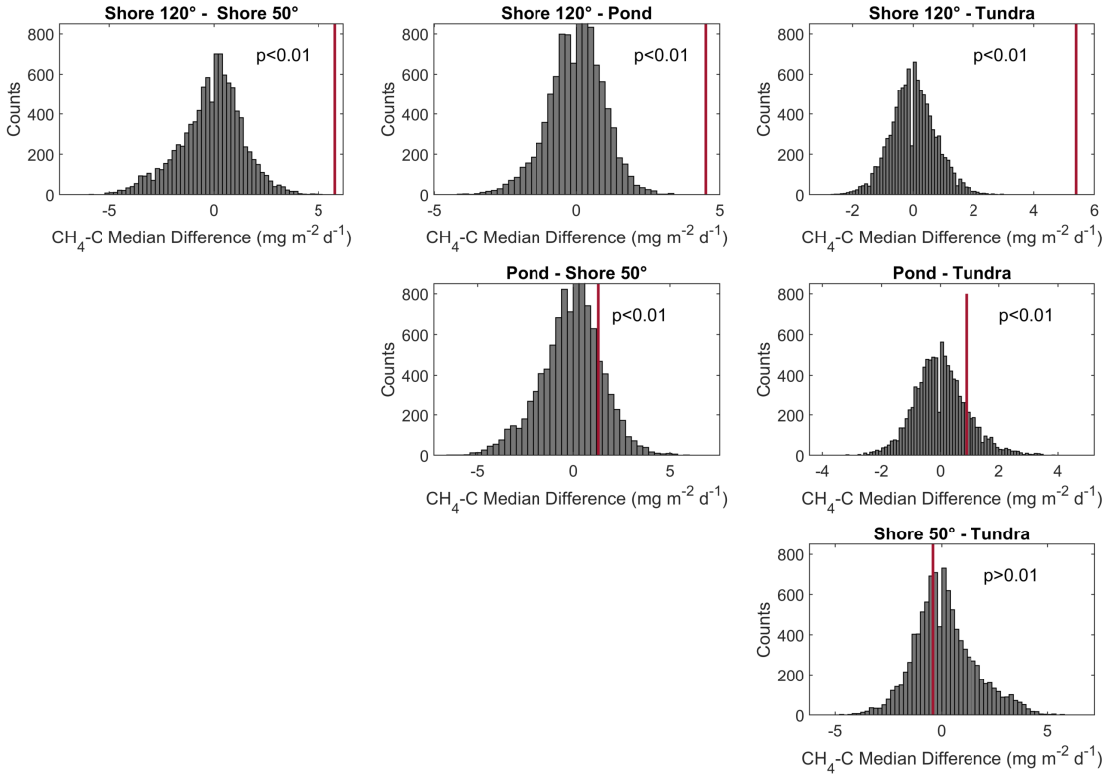

Figure A5. Histogram of permutation tests between the medians of CH_4 emissions from different wind direction classes in figure 6. All medians from flux observations during moderate air temperature conditions. The observed differences in medians between the different wind direction classes are shown in red vertical bars in each plot.

Author contributions. ZR and LK designed the experiments, ZR and LB carried out the fieldwork. ZR, LB, and LK developed the idea for the analysis, and CW and LB prepared the data. The formal analysis and data visualization were performed by LB and ZR with supervision by DH and LK. Resources (land-cover classification) have been provided by CM. LB and ZR prepared the manuscript with contributions from all co-authors.

Competing interests. The authors declare that they have no conflict of interest.

Disclaimer. This study was funded by the Deutsche Forschungsgemeinschaft (DFG, German Research Foundation) under Germany's Excellence Strategy – EXC 2037 'CLICCS - Climate, Climatic Change, and Society' – Project Number: 390683824, contribution to the Center for Earth System Research and Sustainability (CEN) of Universität Hamburg and by the BMBF KoPf project (grant 03F0764A).

Acknowledgements. The authors thank Norman Rüggen for his tireless support before and remotely during the fieldwork, Anna Zaplavnova, Andrei Astapov, and Waldemar Schneider for their equally tireless support in the field, Andrei Astapov and Katya Abramova for additional pictures in the field, Volkmar Assmann and the station crew of Samoylov Island for their logisitical support and Sarah Wiesner, Leonardo Galera, and Tim Eckahardt and for fruitful discussions during the data analysis. Also, the authors thank the reviewers.

References

Abnizova, A., Siemens, J., Langer, M., and Boike, J.: Small ponds with major impact: The relevance of ponds and lakes in permafrost landscapes to carbon dioxide emissions, Global Biogeochemical Cycles, 26, https://doi.org/10.1029/2011gb004237, 2012.

Andresen, C. G. and Lougheed, V. L.: Disappearing Arctic tundra ponds: Fine-scale analysis of surface hydrology in drained thaw lake basins over a 65 year period (1948–2013), Journal of Geophysical Research-Biogeosciences, 120, 466–479, https://doi.org/10.1002/2014jg002778, 2015.

Andresen, C. G., Lara, M. J., Tweedie, C. E., and Lougheed, V. L.: Rising plant-mediated methane emissions from arctic wetlands, Global Change Biology, https://doi.org/10.1111/gcb.13469, 2017.

Bogard, M. J., del Giorgio, P. A., Boutet, L., Chaves, M. C. G., Prairie, Y. T., Merante, A., and Derry, A. M.: Oxic water column methanogenesis as a major component of aquatic CH_4 fluxes, Nature Communications, 5, 5350, https://doi.org/10.1038/ncomms6350, 2014.

Boike, J., Grüber, M., Langer, M., Piel, K., and Scheritz, M.: Orthomosaic of Samoylov Island, Lena Delta, Siberia, https://doi.org/10.1594/PANGAEA.786073, 2012.

Boike, J., Georgi, C., Kirilin, G., Muster, S., Abramova, K., Fedorova, I., Chetverova, A., Grigoriev, M. N., Bornemann, N., and Langer, M.: Temperature, water level and bathymetry of thermokarst lakes in the continuous permafrost zone of northern Siberia - Lena River Delta, Siberia, https://doi.org/10.1594/PANGAEA.846525, 2015a.

Boike, J., Veh, G., Stoof, G., Grüber, M., Langer, M., and Muster, S.: Visible and near-infrared orthomosaic and orthophotos of Samoylov Island, Siberia, summer 2008, with links to data files, https://doi.org/10.1594/PANGAEA.847343, 2015b.

Boike, J., Veh, G., Viitanen, L.-K., Bornemann, N., Stoof, G., and Muster, S.: Visible and near-infrared orthomosaic of Samoylov Island, Siberia, summer 2015 (5.3 GB), https://doi.org/10.1594/PANGAEA.845724, 2015c.

Boike, J., Nitzbon, J., Anders, K., Grigoriev, M. N., Bolshiyanov, D. Y., Langer, M., Lange, S., Bornemann, N., Morgenstern, A., Schreiber, P., Wille, C., Chadburn, S., Gouttevin, I., and Kutzbach, L.: Meteorologic data at station Samoylov (2002-2018, level 2, version 201908), link to archive, PANGAEA, https://doi.org/10.1594/PANGAEA.905232, 2019.

Borrel, G., Jézéquel, D., Biderre-Petit, C., Morel-Desrosiers, N., Morel, J.-P., Peyret, P., Fonty, G., and Lehours, A.-C.: Production and consumption of methane in freshwater lake ecosystems, Research in Microbiology, 162, 832–847, https://doi.org/10.1016/j.resmic.2011.06.004, 2011.

Bouchard, F., Laurion, I., Preskienis, V., Fortier, D., Xu, X., and Whiticar, M. J.: Modern to millennium-old greenhouse gases emitted from ponds and lakes of the Eastern Canadian Arctic (Bylot Island, Nunavut), Biogeosciences, 12, 7279–7298, https://doi.org/10.5194/bg-12-7279-2015, 2015.

Bring, A., Fedorova, I., Dibike, Y., Hinzman, L., Mard, J., Mernild, S. H., Prowse, T., Semenova, O., Stuefer, S. L., and Woo, M. K.: Arctic terrestrial hydrology: A synthesis of processes, regional effects, and research challenges, Journal of Geophysical Research-Biogeosciences, 121, 621–649, https://doi.org/10.1002/2015jg003131, 2016.

Burba, G., Schmidt, A., Scott, R. L., Nakai, T., Kathilankal, J., Fratini, G., Hanson, C., Law, B., Mcdermitt, D. K., Eckles, R., Furtaw, M., and Velgersdyk, M.: Calculating CO_2 and H_2O eddy covariance fluxes from an enclosed gas analyzer using an instantaneous mixing ratio, Global Change Biology, 18, 385–399, https://doi.org/10.1111/j.1365-2486.2011.02536.x, 2012.

Conrad, R.: Contribution of hydrogen to methane production and control of hydrogen concentrations in methanogenic soils and sediments, FEMS Microbiology Ecology, 28, 193–202, https://doi.org/10.1016/S0168-6496(98)00086-5, 1999.

Donis, D., Flury, S., Stöckli, A., Spangenberg, J. E., Vachon, D., and McGinnis, D. F.: Full-scale evaluation of methane production under oxic conditions in a mesotrophic lake, Nature Communications, 8, 1661, https://doi.org/10.1038/s41467-017-01648-4, 2017.

Ducharme-Riel, V., Vachon, D., del Giorgio, P. A., and Prairie, Y. T.: The relative contribution of winter under-ice and summer hypolimnetic CO_2 accumulation to the annual CO_2 emissions from northern lakes, Ecosystems, 18, 547–559, https://doi.org/10.1007/s10021-015-9846-0, 2015.

Edgington, E. and Onghena, P.: Randomization tests, CRC Press, 2007.

Ellis, C. J., Rochefort, L., Gauthier, G., and Pienitz, R.: Paleoecological evidence for transitions between contrasting landforms in a polygon-patterned high arctic wetland, Arctic, Antarctic, and Alpine Research, 40, 624–637, https://doi.org/10.1657/1523-0430(07-059)[ELLIS]2.0.CO;2, 2008.

Encinas Fernández, J., Peeters, F., and Hofmann, H.: On the methane paradox: Transport from shallow water zones rather than in situ methanogenesis is the major source of CH_4 in the open surface water of lakes, Journal of Geophysical Research: Biogeosciences, 121, 2717–2726, https://doi.org/10.1002/2016JG003586, 2016.

Eugster, W., Kling, G., Jonas, T., McFadden, J. P., Wüest, A., MacIntyre, S., and Chapin, F. S.: CO_2 exchange between air and water in an Arctic Alaskan and midlatitude Swiss lake: Importance of convective mixing, Journal of Geophysical Research Atmospheres, 108, https://doi.org/10.1029/2002JD002653, 2003.

Fan, S.-M., Wofsy, S. C., Bakwin, P. S., Jacob, D. J., and Fitzjarrald, D. R.: Atmosphere-biosphere exchange of CO_2 and O_3 in the central Amazon Forest, Journal of Geophysical Research: Atmospheres, 95, 16 851–16 864, https://doi.org/10.1029/JD095iD10p16851, 1990.

Fratini, G., Ibrom, A., Arriga, N., Burba, G., and Papale, D.: Relative humidity effects on water vapour fluxes measured with closed-path eddy-covariance systems with short sampling lines, Agricultural and forest meteorology, 165, 53–63, https://doi.org/10.1016/j.agrformet.2012.05.018, 2012.

Gash, J. H. C. and Culf, A. D.: Applying a linear detrend to eddy correlation data in realtime, Boundary-Layer Meteorology, 79, 301–306, https://doi.org/10.1007/bf00119443, 1996.

Günthel, M., Klawonn, I., Woodhouse, J., Bižić, M., Ionescu, D., Ganzert, L., Kümmel, S., Nijenhuis, I., Zoccarato, L., Grossart, H.-P., and Tang, K. W.: Photosynthesis-driven methane production in oxic lake water as an important contributor to methane emission, Limnology and Oceanography, 65, 2853–2865, https://doi.org/10.1002/lno.11557, 2020.

Hedderich, R. and Whitman, W. B.: Physiology and biochemistry of the methane-producing Archaea, pp. 1050–1079, Springer New York, New York, NY, https://doi.org/10.1007/0-387-30742-7_34, 2006.

Holgerson, M. A. and Raymond, P. A.: Large contribution to inland water CO_2 and CH_4 emissions from very small ponds, Nature Geoscience, 9, 222–226, https://doi.org/10.1038/ngeo2654, 2016.

Holl, D., Pancotto, V., Heger, A., Camargo, S. J., and Kutzbach, L.: Cushion bogs are stronger carbon dioxide net sinks than moss-dominated bogs as revealed by eddy covariance measurements on Tierra del Fuego, Argentina, Biogeosciences, 16, 3397–3423, https://doi.org/10.5194/bg-16-3397-2019, 2019.

Ibrom, A., Dellwik, E., Flyvbjerg, H., Jensen, N. O., and Pilegaard, K.: Strong low-pass filtering effects on water vapour flux measurements with closed-path eddy correlation systems, Agricultural and Forest Meteorology, 147, 140 – 156, https://doi.org/10.1016/j.agrformet.2007.07.007, 2007a.

Ibrom, A., Dellwik, E., Larsen, S. E., and Pilegaard, K.: On the use of the Webb-Pearman-Leuning theory for closed-path eddy correlation measurements, Tellus, Series B: Chemical and Physical Meteorology, 59, 937–946, https://doi.org/10.1111/j.1600-0889.2007.00311.x, 2007b.

Iwata, H., Hirata, R., Takahashi, Y., Miyabara, Y., Itoh, M., and Iizuka, K.: Partitioning eddy-covariance methane fluxes from a shallow lake into diffusive and ebullitive fluxes, Boundary-Layer Meteorology, 169, 413–428, https://doi.org/10.1007/s10546-018-0383-1, 2018.

Jammet, M., Dengel, S., Kettner, E., Parmentier, F.-J. W., Wik, M., Crill, P., and Friborg, T.: Year-round CH_2 and CO_2 flux dynamics in two contrasting freshwater ecosystems of the subarctic, Biogeosciences, 14, 5189–5216, https://doi.org/10.5194/bg-14-5189-2017, 2017.

Jansen, J., Thornton, B. F., Jammet, M. M., Wik, M., Cortés, A., Friborg, T., MacIntyre, S., and Crill, P. M.: Climate-sensitive controls on large spring emissions of CH_4 and CO_2 from northern lakes, Journal of Geophysical Research: Biogeosciences, 124, 2379–2399, https://doi.org/10.1029/2019JG005094, 2019.

Jonsson, A., Åberg, J., Lindroth, A., and Jansson, M.: Gas transfer rate and CO_2 flux between an unproductive lake and the atmosphere in northern Sweden, Journal of Geophysical Research: Biogeosciences, 113, 1–13, https://doi.org/10.1029/2008JG000688, 2008.

Kaimal, J. C. and Finnigan, J. J.: Atmospheric boundary layer flows: their structure and measurement, Oxford university press, 1994.

Kartoziia, A.: Assessment of the ice wedge polygon current state by means of UAV imagery analysis (Samoylov Island, the Lena Delta), Remote Sensing, 11, 1627, https://doi.org/10.3390/rs11131627, 2019.

Kling, G. W., Kipphut, G. W., and Miller, M. C.: The flux of CO_2 and CH_4 from lakes and rivers in arctic Alaska, Hydrobiologia, 240, 23–36, https://doi.org/10.1007/BF00013449, 1992.

Knoblauch, C., Spott, O., Evgrafova, S., Kutzbach, L., and Pfeiffer, E. M.: Regulation of methane production, oxidation, and emission by vascular plants and bryophytes in ponds of the northeast Siberian polygonal tundra, Journal of Geophysical Research-Biogeosciences, 120, 2525–2541, https://doi.org/10.1002/2015jg003053, 2015.

Kormann, R. and Meixner, F. X.: An analytical footprint model for non-neutral stratification, Boundary-Layer Meteorology, 99, 207–224, https://doi.org/10.1023/A:1018991015119, 2001.

Kuhn, M., Lundin, E. J., Giesler, R., Johansson, M., and Karlsson, J.: Emissions from thaw ponds largely offset the carbon sink of northern permafrost wetlands, Scientific Reports, 8, 1–7, https://doi.org/10.1038/s41598-018-27770-x, 2018.

LI-COR: EddyPro Version 7.0.6, 2019.

Liss, P. S. and Slater, P. G.: Flux of gases across the Air-Sea interface, Nature, 247, 181–184, https://doi.org/10.1038/247181a0, 1974.

Lundin, E. J., Giesler, R., Persson, A., Thompson, M. S., and Karlsson, J.: Integrating carbon emissions from lakes and streams in a subarctic catchment, Journal of Geophysical Research: Biogeosciences, 118, 1200–1207, https://doi.org/10.1002/jgrg.20092, 2013.

MATLAB: MATLAB Software 2019b, the MathWorks, Natick, MA, USA, 2019.

Mauder, M. and Foken, T.: Documentation and instruction manual of the eddy covariance software package TK2, Univ, Bayreuth, Abt. Mikrometeorol., ISSN, 161489166, 26–42, 2004.

McGuire, A. D., Christensen, T. R., Hayes, D., Heroult, A., Euskirchen, E., Kimball, J. S., Koven, C., Lafleur, P., Miller, P. A., Oechel, W., Peylin, P., Williams, M., and Yi, Y.: An assessment of the carbon balance of Arctic tundra: Comparisons among observations, process models, and atmospheric inversions, Biogeosciences, 9, 3185–3204, https://doi.org/10.5194/bg-9-3185-2012, 2012.

Moncrieff, J., Clement, R., Finnigan, J., and Meyers, T.: Averaging, detrending, and filtering of eddy covariance time series, in: Handbook of micrometeorology, pp. 7–31, Springer, https://doi.org/10.1007/1-4020-2265-4_2, 2004.

Muster, S., Langer, M., Heim, B., Westermann, S., and Boike, J.: Subpixel heterogeneity of ice-wedge polygonal tundra: a multi-scale analysis of land cover and evapotranspiration in the Lena River Delta, Siberia, Tellus B: Chemical and Physical Meteorology, 64, 17 301, https://doi.org/10.3402/tellusb.v64i0.17301, 2012.

Muster, S., Roth, K., Langer, M., Lange, S., Cresto Aleina, F., Bartsch, A., Morgenstern, A., Grosse, G., Jones, B., Sannel, A. B. K., Sjöberg, Y., Günther, F., Andresen, C., Veremeeva, A., Lindgren, P. R., Bouchard, F., Lara, M. J., Fortier, D., Charbonneau, S., Virtanen, T. A.,

Hugelius, G., Palmtag, J., Siewert, M. B., Riley, W. J., Koven, C. D., and Boike, J.: PeRL: a circum-Arctic Permafrost Region Pond and Lake database, Earth System Science Data, 9, 317–348, https://doi.org/10.5194/essd-9-317-2017, 2017.

Neff, J. C. and Asner, G. P.: Dissolved organic carbon in terrestrial ecosystems: Synthesis and a model, Ecosystems, 4, 29–48, https://doi.org/10.1007/s100210000058, 2001.

Peeters, F., Encinas Fernandez, J., and Hofmann, H.: Sediment fluxes rather than oxic methanogenesis explain diffusive CH_4 emissions from lakes and reservoirs, Scientific Reports, 9, 243, https://doi.org/10.1038/s41598-018-36530-w, 2019.

Ramsar Convention Secretariat: An introduction to the ramsar convention on wetlands (previously The Ramsar Convention Manual), Ramsar Convention Secretariat, Gland, Switzerland, 2016.

Rehder, Z., Zaplavnova, A., and Kutzbach, L.: Identifying drivers behind spatial variability of methane concentrations in East Siberian ponds, Frontiers in Earth Science, 9, 183, https://doi.org/10.3389/feart.2021.617662, 2021.

Repo, M. E., Huttunen, J. T., Naumov, A. V., Chichulin, A. V., Lapshina, E. D., Bleuten, W., and Martikainen, P. J.: Release of CO_2 and CH_4 from small wetland lakes in western Siberia, Tellus, Series B: Chemical and Physical Meteorology, 59, 788–796, https://doi.org/10.1111/j.1600-0889.2007.00301.x, 2007.

Rößger, N., Wille, C., Holl, D., Göckede, M., and Kutzbach, L.: Scaling and balancing carbon dioxide fluxes in a heterogeneous tundra ecosystem of the Lena River Delta, Biogeosciences, 16, 2591–2615, https://doi.org/10.5194/bg-16-2591-2019, 2019a.

Rößger, N., Wille, C., Veh, G., Boike, J., and Kutzbach, L.: Scaling and balancing methane fluxes in a heterogeneous tundra ecosystem of the Lena River Delta, Agricultural and Forest Meteorology, 266-267, 243–255, https://doi.org/10.1016/j.agrformet.2018.06.026, 2019b.

Runkle, B. R., Sachs, T., Wille, C., Pfeiffer, E. M., and Kutzbach, L.: Bulk partitioning the growing season net ecosystem exchange of CO_2 in Siberian tundra reveals the seasonality of it carbon sequestration strength, Biogeosciences, 10, 1337–1349, https://doi.org/10.5194/bg-10-1337-2013, 2013.

Sepulveda-Jauregui, A., Walter Anthony, K. M., Martinez-Cruz, K., Greene, S., and Thalasso, F.: Methane and carbon dioxide emissions from 40 lakes along a north-south latitudinal transect in Alaska, Biogeosciences, 12, 3197–3223, https://doi.org/10.5194/bg-12-3197-2015, 2015.

Sieczko, A. K., Duc, N. T., Schenk, J., Pajala, G., Rudberg, D., Sawakuchi, H. O., and Bastviken, D.: Diel variability of methane emissions from lakes, Proceedings of the National Academy of Sciences, 117, 21 488–21 494, https://doi.org/10.1073/pnas.2006024117, 2020.

Squires, M. M. and Lesack, L. F.: The relation between sediment nutrient content and macrophyte biomass and community structure along a water transparency gradient among lakes of the Mackenzie Delta, Canadian Journal of Fisheries and Aquatic Sciences, 60, 333–343, https://doi.org/10.1139/f03-027, 2003.

Treat, C. C., Marushchak, M. E., Voigt, C., Zhang, Y., Tan, Z., Zhuang, Q., Virtanen, T. A., Räsänen, A., Biasi, C., Hugelius, G., Kaverin, D., Miller, P. A., Stendel, M., Romanovsky, V., Rivkin, F., Martikainen, P. J., and Shurpali, N. J.: Tundra landscape heterogeneity, not interannual variability, controls the decadal regional carbon balance in the Western Russian Arctic, Global Change Biology, 24, 5188–5204, https://doi.org/10.1111/gcb.14421, 2018.

Tuovinen, J.-P., Aurela, M., Hatakka, J., Räsänen, A., Virtanen, T., Mikola, J., Ivakhov, V., Kondratyev, V., and Laurila, T.: Interpreting eddy covariance data from heterogeneous Siberian tundra: land-cover-specific methane fluxes and spatial representativeness, Biogeosciences, 16, 255–274, https://doi.org/10.5194/bg-16-255-2019, 2019.

U.S. Geological Survey, EROS Center: CORONA Satellite Photographs, 1965.

Vickers, D. and Mahrt, L.: Quality control and flux sampling problems for tower and aircraft data, Journal of Atmospheric and Oceanic Technology, 14, 512–526, https://doi.org/10.1175/1520-0426(1997)014<0512:QCAFSP>2.0.CO;2, 1997.

Vonk, J. E., Tank, S. E., Bowden, W. B., Laurion, I., Vincent, W. F., Alekseychik, P., Amyot, M., Billet, M. F., Canário, J., Cory, R. M., Deshpande, B. N., Helbig, M., Jammet, M., Karlsson, J., Larouche, J., Macmillan, G., Rautio, M., Walter Anthony, K. M., and Wickland, K. P.: Reviews and syntheses: Effects of permafrost thaw on Arctic aquatic ecosystems, Biogeosciences, 12, 7129–7167, https://doi.org/10.5194/bg-12-7129-2015, 2015.

Walter, K. M., Zimov, S. A., Chanton, J. P., Verbyla, D., and Chapin, F. S.: Methane bubbling from Siberian thaw lakes as a positive feedback to climate warming, Nature, 443, 71–75, https://doi.org/10.1038/nature05040, 2006.

Walter Anthony, K. M. and Anthony, P.: Constraining spatial variability of methane ebullition seeps in thermokarst lakes using point process models, Journal of Geophysical Research: Biogeosciences, 118, 1015–1034, https://doi.org/10.1002/jgrg.20087, 2013.

Webb, E. K., Pearman, G. I., and Leuning, R.: Correction of flux measurements for density effects due to heat and water vapour transfer, Quarterly Journal of the Royal Meteorological Society, 106, 85–100, https://doi.org/10.1002/qj.49710644707, 1980.

Wik, M., Varner, R. K., Anthony, K. W., MacIntyre, S., and Bastviken, D.: Climate-sensitive northern lakes and ponds are critical components of methane release, Nature Geoscience, 9, 99–105, https://doi.org/10.1038/ngeo2578, 2016.